



**Michigan  
Technological  
University**

Michigan Technological University  
**Digital Commons @ Michigan Tech**

---

Dissertations, Master's Theses and Master's Reports

---

2016

## **AUTONOMOUS DC MICROGRID WITH SELF-CONFIGURABLE FEASIBILITY**

Amir Farshad

*Michigan Technological University, farshad@mtu.edu*


Copyright 2016 Amir Farshad

---

### **Recommended Citation**

Farshad, Amir, "AUTONOMOUS DC MICROGRID WITH SELF-CONFIGURABLE FEASIBILITY", Open Access Master's Thesis, Michigan Technological University, 2016.  
<https://doi.org/10.37099/mtu.dc.etdr/263>

Follow this and additional works at: <https://digitalcommons.mtu.edu/etdr>

 Part of the [Power and Energy Commons](#)

AUTONOMOUS DC MICROGRID WITH SELF-CONFIGURABLE FEASIBILITY

By

Amir Farshad

A THESIS

Submitted in partial fulfillment of the requirements for the degree of

MASTER OF SCIENCE

In Electrical Engineering

MICHIGAN TECHNOLOGICAL UNIVERSITY

2016

© 2016 Amir Farshad

This thesis has been approved in partial fulfillment of the requirements for the Degree of MASTER OF SCIENCE in Electrical Engineering.

Department of Electrical and Computer Engineering

Thesis Advisor: *Wayne W. Weaver*

Committee Member: *Nina Mahmoudian*

Committee Member: *John Lukowski*

Department Chair: *Daniel R. Fuhrmann*

# **DEDICATION**

To my family, friends and teachers



# CONTENTS

<b>LIST OF FIGURES .....</b>	<b>iv</b>
<b>LIST OF TABLES.....</b>	<b>vii</b>
<b>ACKNOWLEDGMENTS.....</b>	<b>ix</b>
<b>ABSTRACT.....</b>	<b>x</b>
<b>CHAPTER 1 INTRODUCTION .....</b>	<b>1</b>
<b>CHAPTER 2 OVERVIEW.....</b>	<b>5</b>
2.1 BACKGROUND AND RELATED RESEARCHES .....	5
2.1.1 AUTONOMOUS DC MICROGRID .....	6
2.1.2 LOAD/SOURCE IDENTIFICATION .....	7
2.1.3 DISTRIBUTED GENERATION (DG) SOURCES AND STORAGE DEVICES .....	10
2.1.4 DC MICROGRID REFERENCE ARCHITECTURES.....	12
2.1.5 EFFICIENCY OF MICROGRIDS.....	15
2.1.6 CONTROL METHODS .....	17
2.2 OBJECTIVES .....	18
<b>CHAPTER 3 LOAD/SOURCE IDENTIFICATION IN AUTONOMOUS DC MICROGRID.....</b>	<b>20</b>
3.1 SOURCE AND LOAD TYPES IN THE MICROGRID .....	20
3.2 BATTERY: VOLTAGE SOURCE OR LOAD.....	21
3.3 DC MICROGRID CONFIGURATION .....	27

3.4 FINITE STATE MACHINE IN REAL-TIME APPLICATIONS .....	29
3.5 PID CONTROLLERS .....	30
3.6 SIMULINK MODEL AND PARAMETER ESTIMATION TOOL .....	33
<b>CHAPTER 4 EXPERIMENTAL APPARATUS AND RESULTS .....</b>	<b>37</b>
4.1 IMPLEMENTING IDENTIFICATION METHOD.....	37
4.1.1 BATTERY STATE OF CHARGE (SOC) TABLE .....	38
4.1.2 LOADS AND SOURCES IN THE CONFIGURED GRID .....	40
4.1.3 DECISION TREE FOR DC MICROGRID WITH DC POWER SUPPLY AND BATTERY	42
4.1.4 EXPERIMENTAL DISCHARGE BEHAVIOR OF THE 12 V BATTERY .....	44
4.2 EMBEDDED COMPUTER CONTROL SYSTEM.....	45
4.3 SIMULINK REAL-TIME .....	49
4.4 SMART MODULE CONFIGURATION.....	50
4.5 EXPERIMENTAL RESULTS.....	53
4.6 TRANSFERRING POWER FROM SOURCE TO LOAD .....	58
4.7 LOAD SHARING.....	60
<b>CHAPTER 5 CONCLUSIONS .....</b>	<b>66</b>
5.1 SUMMARY OF ACCOMPLISHMENTS .....	66
5.2 RECOMMENDATIONS FOR FUTURE WORK .....	67
<b>REFERENCES.....</b>	<b>68</b>
<b>APPENDIX A PARAMETER ESTIMATION RESULTS.....</b>	<b>75</b>
<b>APPENDIX B BATTERY DISCHARGE PROCESS .....</b>	<b>76</b>
<b>APPENDIX C SMART MODULE LAYOUT .....</b>	<b>77</b>
<b>APPENDIX D DETAILED SIMULINK MODELS .....</b>	<b>78</b>
<b>APPENDIX E MATLAB CODE FOR PULLING DATA FROM TARGET PC.....</b>	<b>89</b>

<b>APPENDIX F</b>	<b>POWER BOARD ENERGY EFFICIENCY .....</b>	<b>90</b>
<b>APPENDIX G</b>	<b>VOLTAGE SENSORS CALIBRATION .....</b>	<b>93</b>

# LIST OF FIGURES

<b>2-1:</b> DC microgrid reference architecture with photovoltaic (PV) and Maximum Power Point Tracking (MPPT) "Adapted from [4]" .....	12
<b>2-2:</b> DC Microgrid reference structure with Firm Generation"Adapted from [4]" .....	13
<b>2-3:</b> DC Microgrid reference configuration with PV, MPPT, and battery "Adapted from [4]" .....	14
<b>2-4:</b> Base DC Microgrid configuration .....	15
<b>2-5:</b> Paralleling control methods in DC microgrids "Adapted from [26]" .....	18
<b>3-1:</b> Generic battery model for dynamic simulation in MATLAB R2015a "Adapted from [38]" .....	22
<b>3-2:</b> Discharge curve of 12 V battery.....	24
<b>3-3:</b> Exponential area of 12 V battery discharge curve.....	25
<b>3-4:</b> Simulation Results of Lead-Acid voltage characteristics for (a) Nominal current discharge at 2.5 A (b) Different discharge current rates .....	26
<b>3-5:</b> Simulation results of (a) Voltage, (b) Battery current, and (c) SOC of the battery for three discharge rates (0.5 A, 0.95 A, and 1.7 A).....	27
<b>3-6:</b> The basic schematic diagram of the DC microgrid .....	28
<b>3-7:</b> PID controller scheme implemented for DC microgrid .....	32
<b>3-8:</b> Simulation model of DC microgrid for parameter estimation.....	34
<b>3-9:</b> Estimated parameters in different iterations (a) C1, L, R1, Rc1, Rc2, Rl and Rl2 (b) C2 and L2 .....	34
<b>3-10:</b> Measured data and simulation output by parameter estimation .....	36

<b>4-1:</b> Experimental setup for identification method .....	38
<b>4-2:</b> Simulation results of battery voltage in (a) 100% initial SOC (b) 80% initial SOC (c) 60% initial SOC and (d) 40% initial SOC with constant 53 $\Omega$ resistive load ....	40
<b>4-3:</b> Simulation Decision Tree of identification method and transferring power.....	43
<b>4-4:</b> Experimental discharge rate of 12V battery from (a) 95% SOC to (i) 6% initial SOC.....	44
<b>4-5:</b> PC/104-Plus with three stacked modules - CPU (top), Timer/Counter (middle), and Analog I/O (bottom).....	46
<b>4-6:</b> DC Microgrid configuration.....	50
<b>4-7:</b> Experimental setup of smart module configuration .....	51
<b>4-8:</b> Converter's switches (IGBT) configuration "Adapted from [47]".....	51
<b>4-9:</b> PC/104-Plus connections with Host PC and other parts of power electronics board .....	52
<b>4-10:</b> Simulation result of the tested battery voltage .....	54
<b>4-11:</b> Simulink Real-Time target screen of connecting .....	55
<b>4-12:</b> Battery voltage mean values during the first 20 seconds of connecting the identification resistors.....	56
<b>4-13:</b> Simulink Real-Time target screen of connecting .....	57
<b>4-14:</b> DC power source voltage mean values during the first.....	58
<b>4-15:</b> Transferring power from DC source to LED and DC motor.....	59
<b>4-16:</b> Experimental results of DC Microgrid with LED and DC Motor as load.....	60
<b>4-17:</b> Experimental outputs for load sharing (a) DC Bus voltage (b) Load current from source 1 (c) Load current from source 2 .....	61
<b>4-18:</b> Flowchart diagram of the DC Microgrid control scheme .....	63
<b>4-19:</b> Experimental outputs for load sharing between two batteries (a) DC Bus voltage (b) Load current from source 1 (c) Load current from source 2 .....	65
<b>C-1:</b> Wiring diagram of the Power Electronics panel.....	77

<b>D-1:</b> Simulink model for the parameter estimation .....	78
<b>D-2:</b> Simulink control model used in part 4.6 .....	79
<b>D-3:</b> The sequential logic circuits diagram of the MATLAB state machine in part 4.6 ..	80
<b>D-4:</b> Load identification Simulink model .....	81
<b>D-5:</b> State machine diagram of Chart 1 of the load identification model.....	82
<b>D-6:</b> Real-Time Simulink model in the load sharing experiment.....	83
<b>D-7:</b> Measurement block of the Simulink model for capturing data and presenting on target PC display .....	84
<b>D-8:</b> Real-Time Simulink state machine diagram for matching voltage and transferring power.....	85
<b>D-9:</b> Real-Time Simulink model with the PI controllers in the load sharing experiment .....	86
<b>D-10:</b> Simulink model of the DC grid and state machine controller along with the PI controllers .....	87
<b>F-1:</b> Power board efficiency versus input power.....	91
<b>F-2:</b> Power board efficiency versus output current .....	92
<b>G-1:</b> Voltage gain value of the voltage sensing board versus input voltage .....	94

# LIST OF TABLES

<b>2-1:</b> The main specifications of common microgrid DG sources [5] .....	10
<b>2-2:</b> Characteristics of main storage devices in microgrid [5].....	11
<b>2-3:</b> Peak-load efficiencies of power electronics devices in the microgrid [4] .....	16
<b>3-1:</b> Equation 4-1 parameters descriptions and examined battery parameters .....	23
<b>3-2:</b> Battery specifications .....	25
<b>3-3:</b> Changing simulation model parameters from initial guess to final value by Parameter Estimation Tool and measured parameters.....	35
<b>4-1:</b> Battery voltages for different initial state of charge with two different resistors (White: 53 $\Omega$ , Gray: 5.3 $\Omega$ ) for a 2 minute period.....	39
<b>4-2:</b> Loads and sources for validating identification results .....	41
<b>4-3:</b> Possible loads and sources in DC microgrids .....	41
<b>4-4:</b> PC/104-Plus CPU module specifications.....	47
<b>4-5:</b> Mesa 4I22 Timer/Counter module features .....	47
<b>4-6:</b> Diamond-MM-32DX-AT analog and digital I/O specifications [45] .....	48
<b>4-7:</b> Diamond-MM-32DX-AT 16-Bit Analog I/O .....	48
<b>4-8:</b> Load sharing experimental variables.....	61
<b>4-9:</b> Experimental Parameters of load sharing between batteries.....	64
<b>A-1:</b> Simulation model's parameters changing in iterations .....	75

<b>D-1:</b> Block parameters of Lead-Acid battery model in MATLAB/Simulink.....	88
<b>F-1:</b> Power electronics board efficiency in different voltage and current levels.....	90



# ACKNOWLEDGMENTS

I would like to thank my advisor Dr. Weaver for all the support, encouragement and technical guidance throughout my studies in Michigan Tech University.

I would like to express my appreciation to my committee members Prof. Mahmoudian and Prof. Lukowski for their time and helpful comments.

I am grateful for all of the help and support that my graduate school colleagues provided over the years. I would especially like to acknowledge Shishirkumar Patel, Mehrzad Bijaieh and Sashank Narayan.

Finally, I would like to thank my parents, sisters and brother for their support throughout my entire life.

# ABSTRACT

Microgrids are power systems that work not only from the main power grid, but also in island mode operation. As each of the power sources and loads have voltage and current limitations, the autonomous microgrid should be able to control voltage and current levels while loads and sources are connected to the grid. Therefore, the microgrid bus voltage remains constant and power transfers safely.

To configure an autonomous microgrid, the load and source type identification comes to mind. An autonomous microgrid needs to know the type of the electrical components which are going to be connected to the grid. In this study, by using voltage trend recognition, the type of the electrical device (DC power supply, battery, and load) is identified. Moreover, by recognizing the battery state of charge (SOC), the electrical power management of the microgrid is optimized.

The experimental setup is able to detect the type of the electrical device (battery, voltage source or load) and then configures the DC microgrid to transfer power efficiently.

By implementing PI controller and fuzzy method to control the DC microgrid, various cases in the microgrid such as load sharing, charging the battery, powering the different loads (uncharged battery, DC motor, and resistive loads) and importing new sources and

loads are used to test the experimental setup of the DC microgrid and related power electronics converters. The experimental results demonstrate the validity and efficiency of the proposed system for the self-configurable autonomous DC microgrid.

# **CHAPTER 1**

## **INTRODUCTION**

The microgrid concept refers to the connection of multiple sources of electrical energy (DGs, storage units, national grid, etc.) with different types of loads (residential consumers, Electric Vehicles (EV), data centers, uncharged batteries, etc.) [1-3]. Most of the Distributed generator (DG) sources have been equipped with power electronics converters to make the microgrid effective and controllable. As each of the microgrid components works at different voltage levels and types (AC or DC), power electronics devices make it possible to connect all of them together as a grid. By this configuration of an electrical grid, microgrids have the ability to increase not only the reliability and safety of the power grid, but also the power quality [4, 5].

The AC power transfer is traditionally the main power delivery option in the electrical grid as AC enables high power transmission over very long distances. As the length of the transmission lines increases, the efficiency of transferring power and also the capacity of transmission lines decreases. The main way to improve the efficiency of transmission lines

is by increasing the voltage level. In the past, only AC networks were able to boost the voltage level through the transformer [6]. However, the technology advances in the field of power electronics and high power switches led to the efficient AC to DC and DC to DC converters. The increasing usage of the DC grids is related to both the ability of high-power DC converters for long-distance power transmission and local DC generation sources and DC loads (data centers, electrical vehicles, air conditioning, building communications, etc.) [4, 7].

Different architectures of a microgrid (AC microgrid, DC microgrid or hybrid AC/DC microgrid) depend on both source and load types. For each type of microgrid, there are some reference architectures according to the levels of reliability, power quality improvement, and power flow direction.

The dynamic behavior and control system of such a microgrid play an important role in the safety and reliability of supplying energy to consumers. The electrical parameters that are usually implemented for control theories are voltage, current and power (real and reactive for AC systems). The aim of the controlling method is to distribute power from different sources to various loads in the most efficient and reliable way. Moreover, the controlling method should be able to take control of the power electronics interfaces which are connected to the Point of Common Coupling (PCC) of the loads and sources [4, 8, 9].

One of the applications of the microgrid is powering loads in an island mode operation when there is a power electric outage in the main grid. In this case, the microgrid regulates

the use of available DG sources to supply energy for loads. Additionally, the microgrid makes it possible to import/export new loads and sources into the grid [1].

The work proposed in this thesis is to detect the type of electrical source or load which is to be connected to the grid autonomously, without prior knowledge of the device. In this case, after detecting the load or source type, the power electronics interface makes it possible to then supply power to the load side. In this manner, the grid is formed with an unknown source without the need for a human operator or prior information about the source and load characteristics.

In Chapter 2 of this thesis, the definition and the properties of the autonomous microgrid will be discussed. Moreover, common DG sources in the microgrid will be presented and the different topologies of microgrids will be provided. The load and source identification theory and methods are reviewed in this chapter, followed by the objectives of this project in the last part.

Chapter 3 investigates the proposed load/source identification method for an autonomous DC microgrid. The battery voltage behavior at different discharge rates is studied and the main idea of the proposed identification system is presented. The DC/DC converter topology is introduced and state equations are provided. Finite state machine and PID controller are introduced in this chapter and their real-time applications are studied. The detailed simulation model is presented and then, a parameter optimization tool is used to update the parameters of the model.

Chapter 4 presents the details about experimental apparatus and results. First, the implementation of the proposed identification method is presented. Different parts of the smart module, which make an autonomous DC microgrid, are presented in Chapter 4. Moreover, the experimental results for load/source identification system, load sharing, and distributing power are presented.

The conclusion of this project and proposed future works are provided in Chapter 5. The results from both the simulation and the experimental setup are presented. Lastly, conclusions and future works are suggested.

# **CHAPTER 2**

## **OVERVIEW**

The motivation of this thesis is to make an autonomous DC microgrid with load/source identification method. The type of the electrical components is detected and by using a smart module as a connector between sources and loads, an autonomous microgrid is developed. In this chapter, the previous works around autonomous microgrids and load/source identification are provided and then the objectives of this thesis are presented.

### **2.1 BACKGROUND AND RELATED RESEARCHES**

In this section, a literature review about different topics is presented. The autonomous DC microgrid concept and different load/source identification are introduced. Different DC microgrid configurations and control schemes for microgrid management are provided here from various resources.



### **2.1.1 AUTONOMOUS DC MICROGRID**

A microgrid is an electrical subsystem which consists of a number of distributed energy resources in connection with a cluster of loads. The most notable merit of the idea of using microgrids is the availability of lower cost of operation. Furthermore, microgrids dramatically increase the overall reliability of the system which is also worth millions of dollars [10, 11].

The sources of electrical energy need to be equipped with power electronics interfaces and control schemes to be able to make a stable microgrid. The main advantage of a microgrid is that it can act as an aggregated controllable system and could operate as a single power grid. In other words, the microgrid has the ability to work autonomously by configuring the grid from available sources and loads. In this operation mode, which is also named island mode operation, local loads and sources make an island which is disconnected from the main grid. For example, if a fault or maintenance occurs which disrupts the main grid, consumers can receive continuous power from locally distributed energy resources. Moreover, in the case of poor power quality from the main grid, the microgrid can be islanded and autonomously provide electrical energy for loads [1, 5].

In the control area, there is controversy among different scientists about the idea of using DC microgrids instead of those operated in AC mode. The first advantage of DC microgrids in terms of controlling, is the simple droop control with respect to AC ones. While the bus voltage and currents are tracked in a DC microgrid, an AC microgrid controls both the

frequency and phase of the voltage. Moreover, a DC microgrid would be more efficient as most loads and many sources are DC, thus eliminating the need for multiple conversion steps [12, 13].

### **2.1.2 LOAD/SOURCE IDENTIFICATION**

A DC microgrid consists of different types of sources and loads with various types of electrical devices and different dynamic behaviors. In [14], Calamero, Beck, and Shmilovitz proposed a method of identifying loads in the grid. They analyzed the main current and used both physical components and Z-transform, then utilized the abnormal conditions in the current waveform to identify the load type. The drawback of this method is that it needs special smart meters and power monitors which could be cost prohibitive. Some other identification methods focused on pattern identification of the load power profile [15-18]. There are some load identification studies based on the wavelet of the power and fuzzy logic method [19-21]. The current and voltage waveforms contain a lot of information about the load. There has been work on load identification by Fast Fourier Transform (FFT) and measuring harmonic impedances of load current and voltage [14]. In all of the above methods, the current, voltage and power of the load (or each of them) are analyzed in time or frequency domain for the load identification method. Some of them only use the present measurement devices (voltage and current sensors or power quality measurement devices) but for some others, the new accurate and complete modules need to be added to the system.

The aforementioned studies about load identification, usually are used in online energy managements of the microgrid. In these applications, the central controller of the microgrid uses the information from loads to manage the microgrid during situations such as energy imbalance or peak-load hours. Moreover, in some cases, the management system keeps microgrids operable by disconnecting some of the loads which are inessential in the case of overload demand [22].

In all of the above studies, the loads are connected to the grid and absorb power from the microgrid. Meanwhile, the identification method works to determine the load type or any changes in it. Essentially, all of these systems are online methods for detection of load type during power transfer. According to the load types and behavior, an identification method must be trained and tested before being used in the microgrid system.

In this thesis, the self-configurable microgrid is studied. To achieve this goal, the system should be able to identify electrical components before connecting to the grid. This needs an offline method to first detect the type of the load/source and then makes an autonomous microgrid. Unlike most mentioned methods, the online measurement of the load/source voltage, current, and power, while operating under normal working conditions in the microgrid are not available. In this study, the identification method based on voltage trend is proposed. This method is able to identify battery, DC power supply and load from each other by measuring terminal voltages and analyzing the behavior of voltage in less than a minute. For these types of the load and source studied, time domain analysis of the voltage works fine. Moreover, a study of the voltage trend of the battery and DC supply shows a

significant difference between the terminal voltage of the battery and DC source right after load connection.

Another advantage of the proposed identification method compared to the other aforementioned methods, is the low power property. It means that the identification method does not need to reach the rated current of the power source. It only needs to track the voltage trend of the power source with less than 10% of the rated current. As mentioned before, one advantage of this process is that it takes less than a minute. Low losses and good response time are another advantages of this identification system.

The next advantage of the proposed system is that it doesn't need to add new data acquisition modules to the current setup of the smart module to make the DC microgrid. Furthermore, as long as it works on the time domain analysis of voltage, further computations on data such as FFT and wavelet, which take more time and calculation are irrelevant.

In Chapter 3, more details about the identification method are presented. Additionally, simulation results of the voltage trend analysis on the battery shows the ability of this system for load/source identification. Chapter 4 also provides the experimental results of implementing this method for configuring an autonomous DC microgrid.

### 2.1.3 DISTRIBUTED GENERATION (DG) SOURCES AND STORAGE DEVICES

A microgrid can take advantage of all DG technologies from solar PV and a wind turbine to synchronous generators connected to IC engines. Moreover, combined heat and power (CHP) which generates thermal energy and electricity in an integrated system can also be involved in microgrid systems. Table 2-1 shows the commonly used source of DG and the main characteristic for each of them [5, 23].

**Table 2-1:** The main specifications of common microgrid DG sources [5]

	<b>Solar</b>	<b>Wind</b>	<b>Microhydro</b>	<b>Diesel</b>	<b>CHP</b>
<b>Availability</b>	Geographical location dependent	Geographical location dependent	Geographical location dependent	Any time	Dependent on source
<b>Output Power</b>	DC	AC	AC	AC	AC
<b>Control</b>	Uncontrollable	Uncontrollable	Uncontrollable	Controllable	Dependent on source
<b>Typical Interface</b>	Power electronics converter (DC-DC-AC)	Power electronics converter (AC-DC-AC)	Synchronous or Induction generator	None	Synchronous generator

Storage devices play an important role in the successful operation of the microgrid. These devices balance the energy demand with generation mismatch, at least for short periods of

operation. Fuel cells and microturbine sources have large time constants in the transient state which cause some stability issues for islanded microgrids. The storage devices in a microgrid inject power to the microgrid during the transient time of the aforementioned sources. Some of the main storage technologies are batteries, flywheels, and supercapacitors. Table 2-2 shows these storage devices and some of the related features [5, 24].

**Table 2-2:** Characteristics of main storage devices in microgrid [5]

	<b>Battery</b>	<b>Flywheel</b>	<b>Supercapacitor</b>
<b>Continuous Power (W/kg)</b>	50-100	200-500	500-2000
<b>Typical Backup Time</b>	5-30 min	10-30 sec	10-30 sec
<b>Losses at Standby</b>	Very low	Variable	High
<b>Maintenance</b>	Yearly	Every 5 years	None
<b>Charging Efficiency (%)</b>	75-95	90	85-95
<b>Current Energy Price (\$/kWh)</b>	150-800	3000-4000	4000-5000
<b>Service Life (year)</b>	5	20	>10

## 2.1.4 DC MICROGRID REFERENCE ARCHITECTURES

Figures 2-1 through 2-3 show different base architectures of DC microgrids. In Figure 2-1, photovoltaic (PV) cells inject power to the DC bus through the DC-DC converter. Meanwhile, the grid not only feeds load power to the DC bus through the AC-DC converter, but it also absorbs the excess power of the PV through the DC to AC converter. This power is stored in storage devices of the grid or even supplies power to extra loads of the grid. Both small and large loads could connect to the grid as long as the DC to DC voltage converter modifies the required voltage levels of loads.

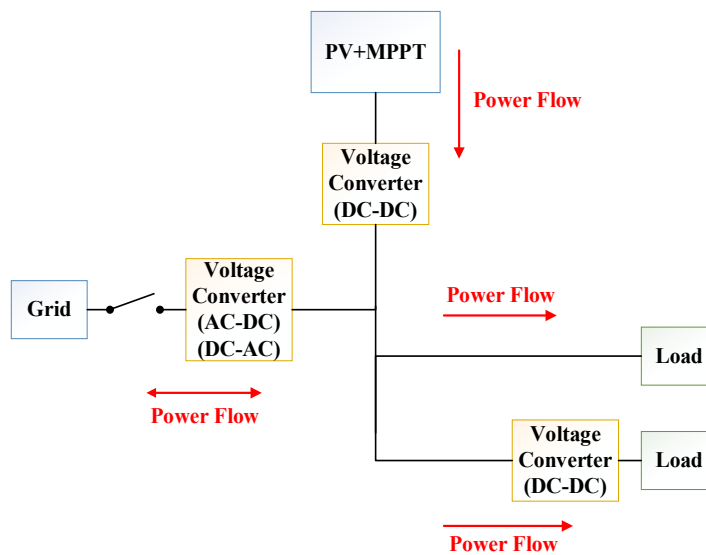


**Figure 2-1:** DC microgrid reference architecture with photovoltaic (PV) and Maximum Power Point Tracking (MPPT) "Adapted from [4]"

Firm Generation refers to electric power guaranteed to be available during the period covered by an agreement. In the case that Firm Generation (generators, wind farms, etc.)

is responsible as one source of supplying energy instead of PV, the AC to DC converter connects that to the DC bus.

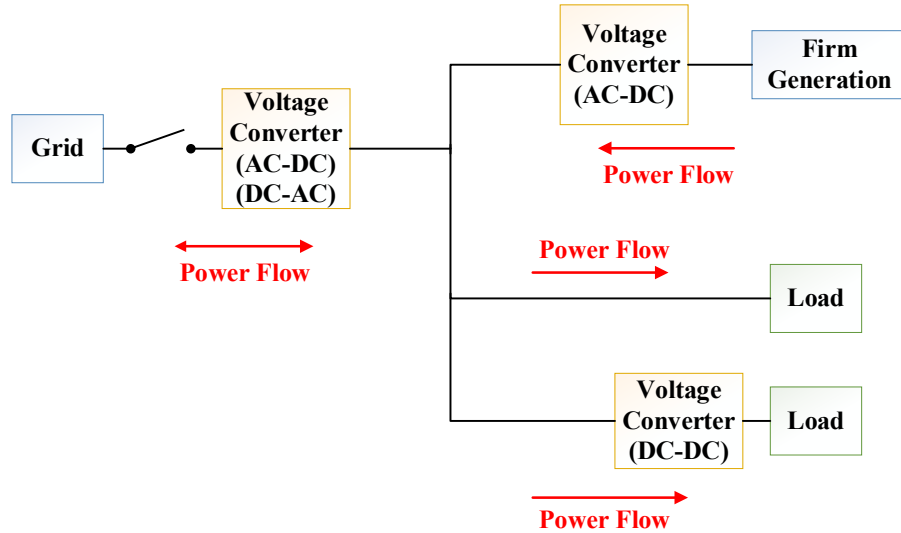


**Figure 2-2:** DC Microgrid reference structure with Firm Generation "Adapted from [4]"

Both the previous DC microgrid configurations suffer from the lack of storage devices. By adding a storage device such as a battery as presented in Figure 2-3, the DC microgrid can keep and use energy for supplying loads. A battery could be charged through PV and also inject electrical energy to the DC grid. There is also the possibility of transferring energy from the battery to the grid if necessary.



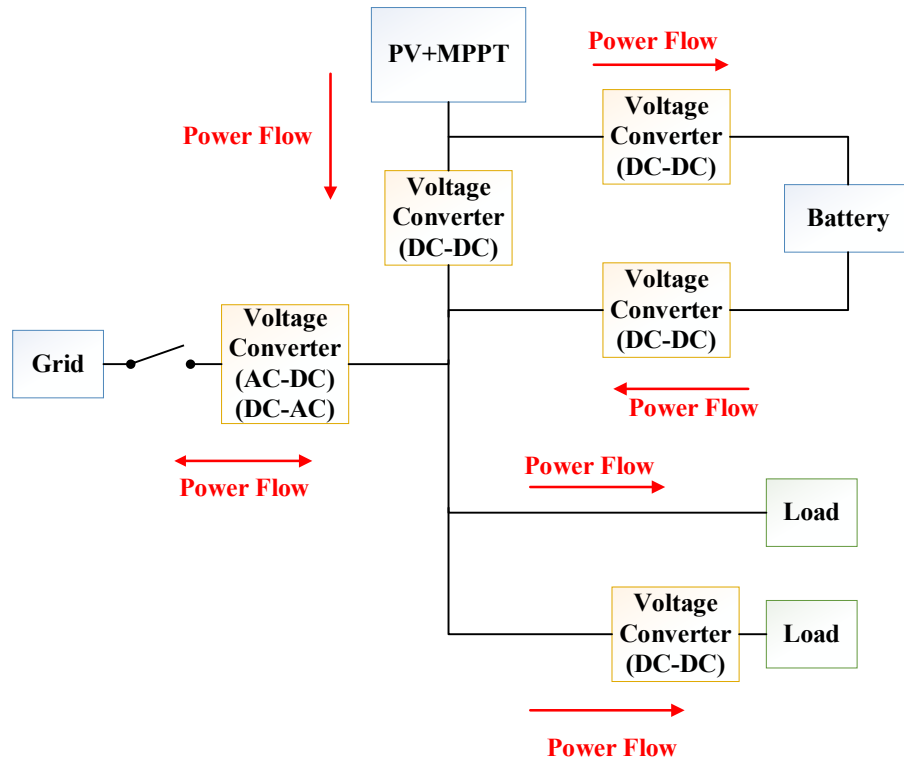


**Figure 2-3:** DC Microgrid reference configuration with PV, MPPT, and battery "Adapted from [4]"

A DC microgrid configuration used in this thesis for both simulation and experimental results is presented in Figure 2-4. The power electronics converter mounted between DC bus and both sources and loads, controls voltage, current and power. The power comes from two different kinds of power supplies; battery and DC power supply which are connected to the electricity grid. The battery serves as a load when it charges from the DC bus. The power flow directions show the possible importing/exporting power to/from loads and sources.

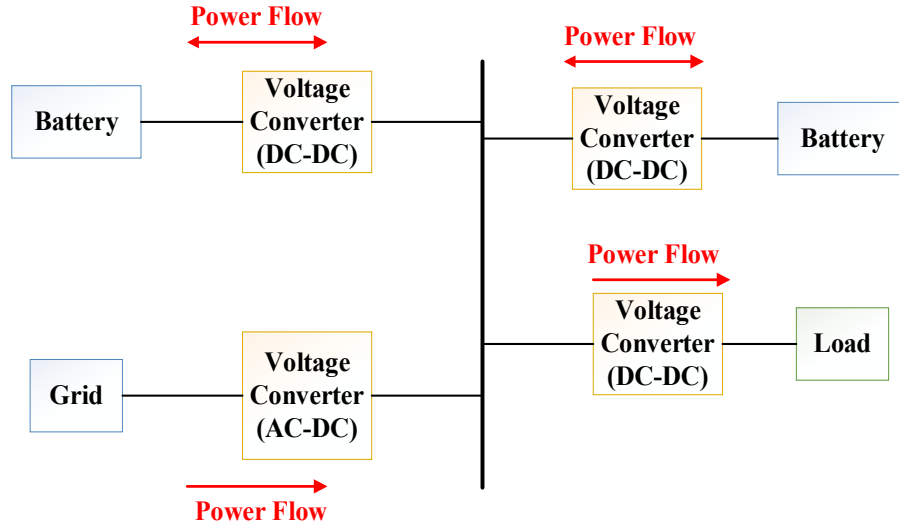


**Figure 2-4:** Base DC Microgrid configuration

### 2.1.5 EFFICIENCY OF MICROGRIDS

A DC system is usually a three conductor system, +DC, -DC, and neutral. By considering the balanced load between positive and negative polarities, and the neutral conductor to be the same as the positive and negative conductors, all conductors in the DC microgrids have the same size. However, the three phase ( $3\phi$ ) AC system is typically a four wire power system. Three phase conductors and neutral conductor are the same size. The main difference between AC and DC systems in terms of conductor size is the flow of reactive power in the system. As the power factor (PF) is always less than 1, the reactive power flow in an AC system occupies some part of the conductors' current limits and increases the size. The total conductor loss mainly relates to the configuration of the microgrid

(which affects the length of the conductor) and the types of the loads (DC or AC) which connect to the grid at the same time [4].

Besides the conductors, power electronics converters and transformers are other main sources of losses in microgrids. The power electronics device efficiency is related to the loading of the device. Table 2-3 shows the peak-load efficiency, which is the efficiency of the converter near the designed maximum load of power electronics devices in a microgrid. This efficiency is near the peak efficiency of the converter [4, 25].

**Table 2-3:** Peak-load efficiencies of power electronics devices in the microgrid [4]

<b>Input Voltage</b>	<b>Output Voltage</b>	<b>Power</b>	<b>Value</b>	<b>Used For</b>
DC High	DC High	High	97.6%	MPPT, Charge controller
DC High	DC Low	Low	96%	DC bus to small loads
DC High	AC High	High	97.6%	Battery or PV to AC bus
AC High	DC High	High	96.5%	AC bus to large DC loads
AC High	AC Low	High	98.5%	AC 480 V-120 V transformer
AC High	DC Low	Low	95%	AC bus to small DC loads

### **2.1.6 CONTROL METHODS**

There are several different control schemes for voltage management of a microgrid [26]. In the Master-Slave method, one of the source converters is responsible for controlling the DC bus voltage and setting the power reference for the other sources. This method requires fast communication between sources and loads. As it is not possible in all cases, droop-control is proposed. By considering the common voltage droop control in the DC microgrid, the DC bus voltage linearly decreases if the current or power of the converter increases. In this method, there is no need for fast communication between sources and loads, and only DC bus voltage is measured [27, 28].

The droop control can be used to not only control the DC bus voltage of the grid, but also provide the load sharing feasibility and power flow management [29, 30]. The other methods could be a combination of different methods and are classified in Figure 2-5.

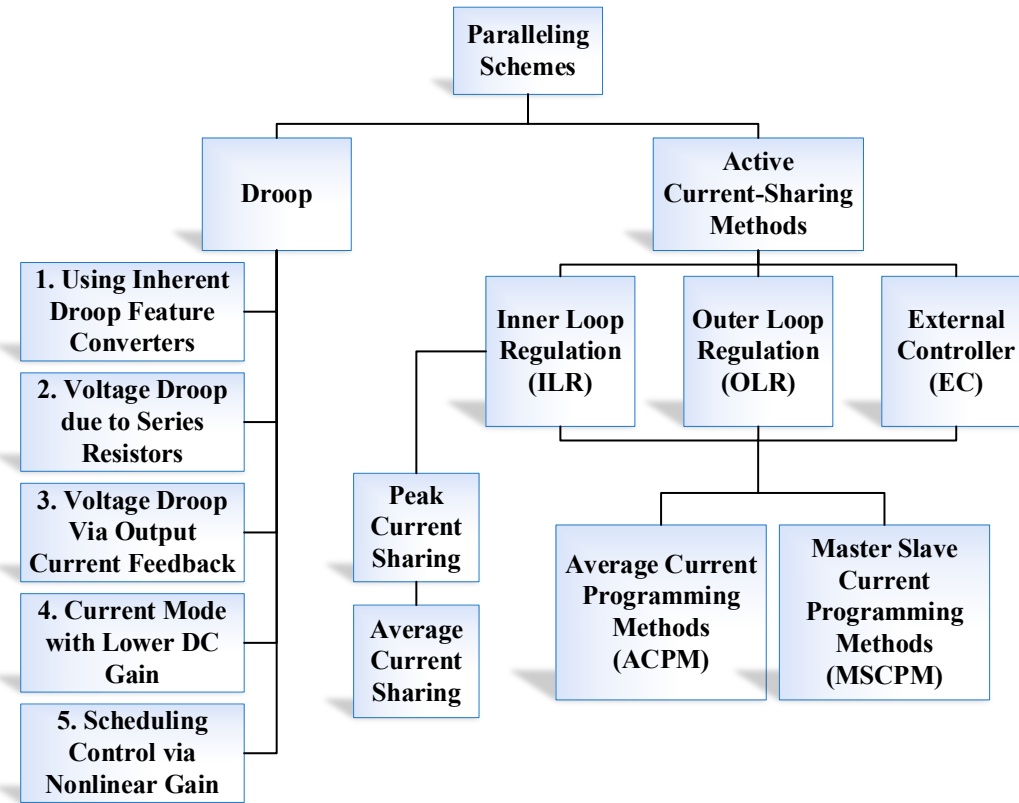


**Figure 2-5:** Paralleling control methods in DC microgrids "Adapted from [26]"

## 2.2 OBJECTIVES

As mentioned in 2.1.1, an autonomous microgrid using available sources and loads, makes a single power grid. Considering that there are some sources and loads in a desert without any prior connection and even knowledge about the type of electrical equipment. Furthermore, there is no access to the proficient operator at that time and location, and constructing the grid in the shortest possible time is the first priority.

First of all, the type of electrical component should be recognized. This needs an identification system for sampling voltage and/or current of the unknown devices. Then, by using trend recognition and analyzing sampled data, the type of the load/source would be identified. In this stage, the identification system needs to be accurate and has the lowest possible energy losses.

The second part of making an autonomous microgrid is the physical connection between sources and loads. To make a stable and efficient microgrid, the bus voltage of the microgrid should maintain a constant voltage. Since each of these sources may produce different voltages, the power electronics converters are applied between sources and loads. By means of these converters, voltage levels are changed to achieve the desired goals.

The next step is controlling the power converter. According to the voltage and current sensors measurements, the control unit of the system produces switching functions for power electronics devices. The power electronics board, computer system, contactors, passive elements, and voltage sensors make up a smart module which is able to control the microgrid. The smart module changes the PWM switching of the converter and produces the desired output voltage. By matching voltage levels of all sources and loads together, the microgrid is established.

Finally, the main goal of transferring power from sources to loads is achieved. The smart module is able to control the transferred power in terms of current, power, and time. The control system considers the limitations of the grid, import/export sources, and loads according to the pre-planned scheme.

## **CHAPTER 3**

### **LOAD/SOURCE IDENTIFICATION IN AUTONOMOUS DC MICROGRID**

In this chapter, the concept of the load/source identification based on voltage trend is studied. The battery being one of the power supply and storage devices in a microgrid, is considered for source identification according to voltage behavior. Next, control schemes for this project and the simulation models are presented.

#### **3.1 SOURCE AND LOAD TYPES IN THE MICROGRID**

For making a self-configurable grid, the importance of detecting sources and loads becomes vital. In this study, two types of sources are considered; a battery and a DC Switching Mode Power Supply (SMPS). Furthermore, different types of loads are also used in the DC microgrid: resistive load, LED light, DC motor, and discharged battery. It is important to

point out that a battery in a DC microgrid is a storage device and can serve as a source or load at different times and conditions.

Autonomous detection of the load or source type helps in configuring the grid and low/high side detection of the boost converter. In addition, the current flow direction is determined according to the role of the connected component to the microgrid. For example, a discharged battery is considered as a load and a charged battery can serve as the DC source.

### **3.2 BATTERY: VOLTAGE SOURCE OR LOAD**

A Valve-Regulated Lead-Acid (VRLA) battery is used for the experimental setup and simulation of the proposed identification method. The voltage across the battery's terminals dynamically varies as a load is connected and draws discharge current from the battery. The electrical models of VRLA batteries are usually composed of the voltage sources, resistors and capacitors [31-34].

The simple electrical model of the battery is an ideal voltage source in series with an internal resistance. One of the drawbacks of this model is that the state of charge (SOC) is not considered. Shepherd developed an equation to model the battery behavior according to SOC, discharge current, internal resistance, and battery voltage [35].



$$E = E_s - K \left( \frac{Q}{Q - it} \right) i - Ni + A \exp(-BQ^{-1}it) \quad (3-1)$$

Where  $E$  is the potential of the cell at time  $t$  during discharge,  $N$  is the internal resistance per unit area,  $K$  is polarization coefficient,  $Q$  is the available amount of active material,  $A$  and  $B$  are empirical constants, and  $E_s$  is a constant potential.

A disadvantage of Shepherd's model is that it gets stuck in an algebraic loop. The generic model of the battery for the dynamic solution that uses SOC as a state variable and does not make an algebraic loop, is proposed by using modified Shepherd's equation [36, 37]. A generic battery model provided in MATLAB R2015a whose equivalent circuit is presented in Figure 3-1, is used for simulation and has the following equation for a Lead-Acid battery in the discharging mode.

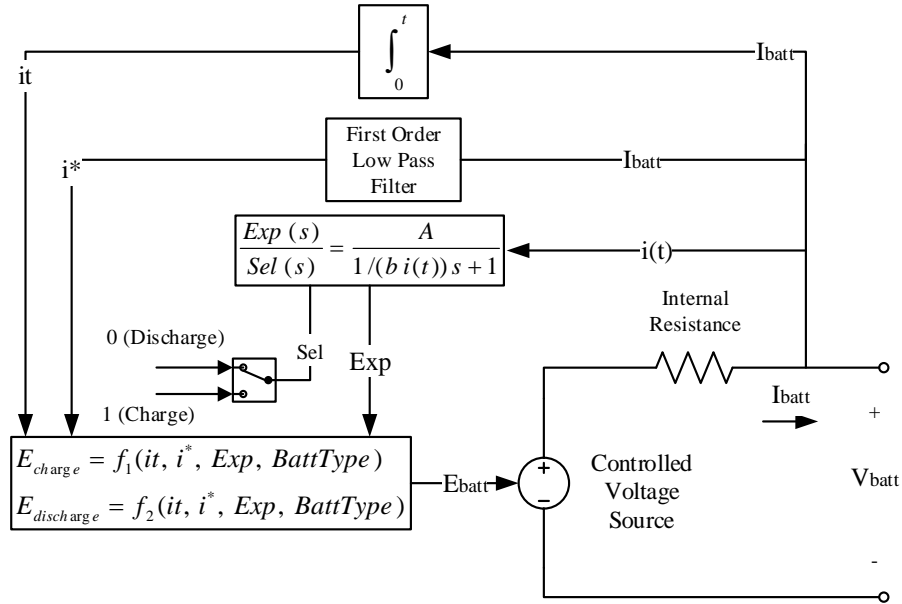


**Figure 3-1:** Generic battery model for dynamic simulation in MATLAB R2015a "Adapted from [38]"

$$f_1(it, i^*, i, Exp) = E_0 - K \cdot \frac{Q}{Q - it} \cdot i^* - K \cdot \frac{Q}{Q - it} \cdot it + Laplace^{-1} \left( \frac{Exp(s)}{Sel(s)} \cdot 0 \right) \quad (3-2)$$

The parameters of the above equation respective to the examined battery are presented in Table 3-1. The battery model is a nonlinear controlled voltage source in series with an internal resistance. By using this model, the exponential part of the discharge characteristic is considered. This exponential behavior of the battery voltage is used for load/source identification as it is decreasing in a short period of time. The discharge curve of the 12 V battery is presented in Figure 3-2. The discharge curve starts from fully charged voltage and decreases to zero volts.

**Table 3-1:** Equation 4-1 parameters descriptions and examined battery parameters

$E_{Batt}$	Nonlinear voltage (V)	-
$E_0$	Constant voltage (V)	12.3709
$Exp(s)$	Exponential zone dynamics (V)	-
$Sel(s)$	Represents the battery mode $Sel(s) = 0$ during battery discharge $Sel(s) = 1$ during battery charging	0
$K$	Polarization constant ( $Ah^{-1}$ ) or Polarization resistance ( $\Omega$ )	0.026195
$i^*$	Low frequency current dynamics (A)	-
$i$	Battery current (A)	2.5
$it$	Extracted capacity (Ah)	-
$Q$	Maximum battery capacity (Ah)	10
$A$	Exponential voltage (V)	0.6666
$B$	Exponential capacity ( $Ah)^{-1}$	90

The Exp(s) transfer function in Figure 3-1 shows that when the battery is discharging, the battery voltage immediately decreases exponentially. In Figure 3-3, the exponential area of discharging curve is demonstrated. It is evident that the terminal voltage of the battery declines rapidly during the first 40 seconds of discharging process.

The parameters of Lead-Acid battery model in MATLAB/Simulink are presented in Table D-1 in Appendix D. Each battery has its specific discharge characteristics and the MATLAB model is tuned according to the individual battery datasheet specifications [38].

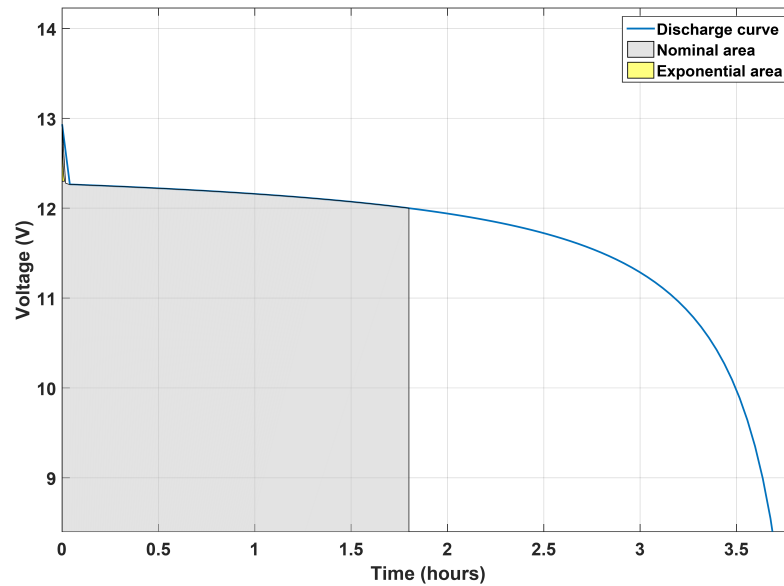


**Figure 3-2:** Discharge curve of 12 V battery

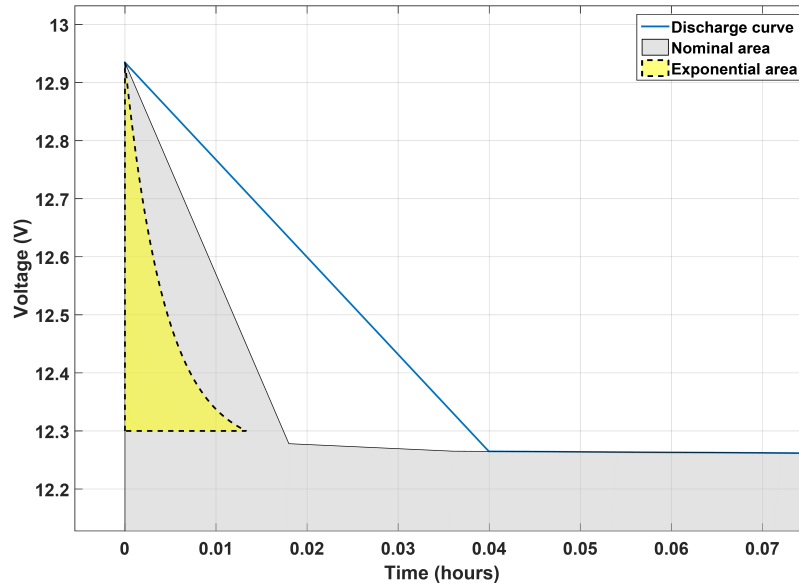


**Figure 3-3:** Exponential area of 12 V battery discharge curve

The discharging behavior of the 12 V battery introduced in Table 3-2, from the simulation is shown in Figure 3-4 and Figure 3-5. In Figure 3-4, the discharge characteristics of this battery according to the MATLAB model and datasheet information are presented. These characteristics match those in the datasheet. The simulation results for three of these discharging rates are shown in Figure 3-5.

**Table 3-2:** Battery specifications

Nominal Voltage	12 V
Nominal Capacity	10.0 Ah @ 20 hours
Internal Resistance	<17 m $\Omega$

In Figure 3-3, the exponential parts of these charts are used for the proposed identification method. The battery terminal voltage first decreases exponentially for a short period of time ( $< 1$  minute), reaches steady state for a while, and then drops to zero. Meanwhile, the battery's state of charge (SOC) also decreases.

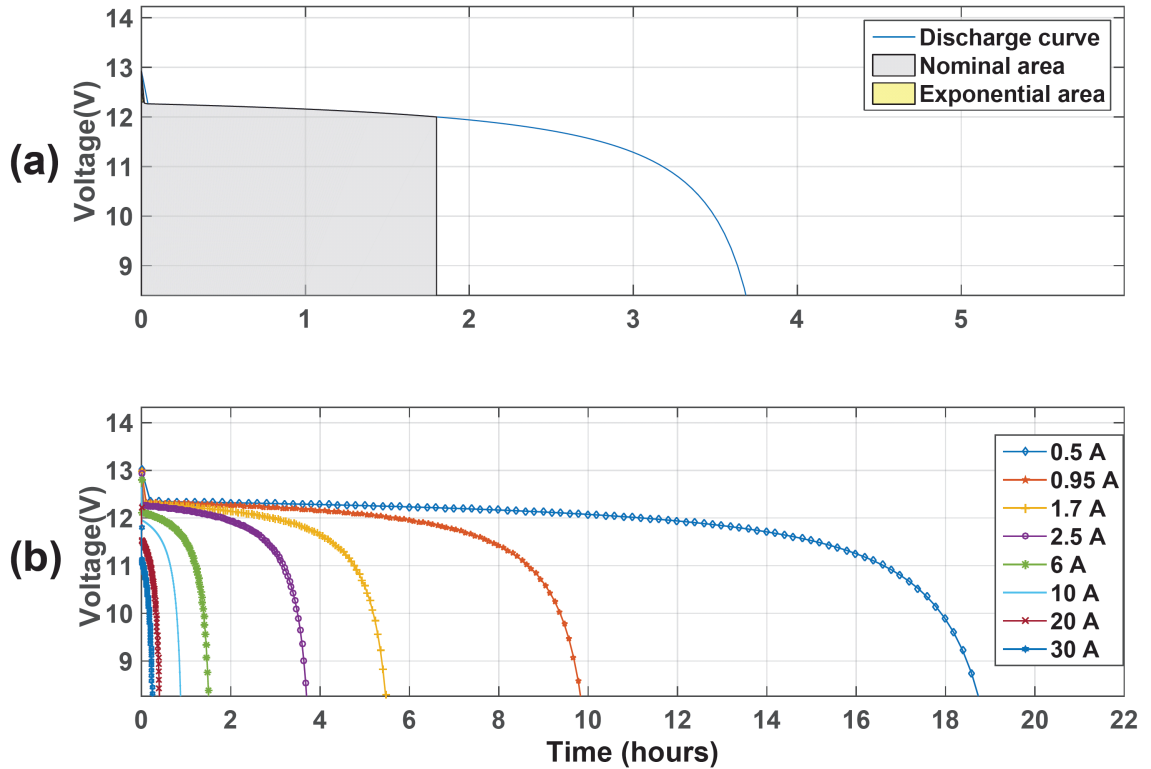


**Figure 3-4:** Simulation Results of Lead-Acid voltage characteristics for  
(a) Nominal current discharge at 2.5 A (b) Different discharge current rates

A DC power supply, which converts AC voltage to DC, has an almost constant output voltage level while connected to the load. It may have some variations, but these oscillations are not predictable and systematic. It means that the power supply output may

have some increasing and decreasing trends around steady state value, but not in an exponentially decreasing manner.

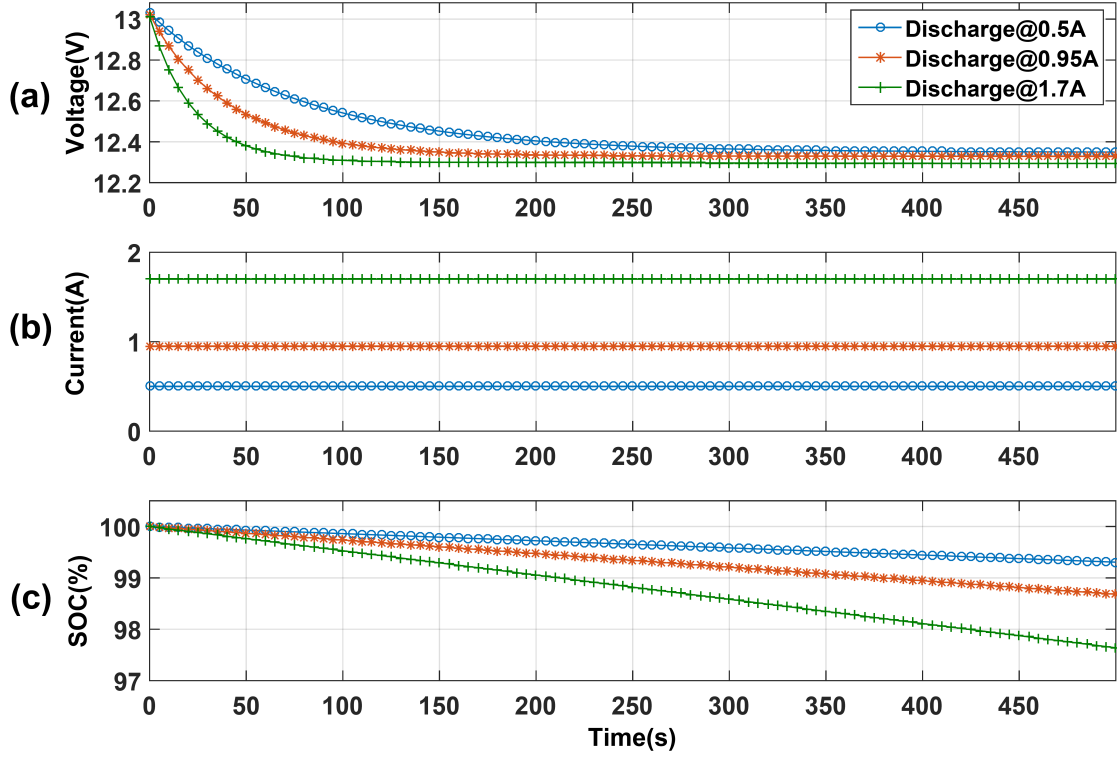


**Figure 3-5:** Simulation results of (a) Voltage, (b) Battery current, and (c) SOC of the battery for three discharge rates (0.5 A, 0.95 A, and 1.7 A)

### 3.3 DC MICROGRID CONFIGURATION

The basic DC microgrid scheme for setup and investigation is presented in Figure 3-6. It consists of one source which is connected through a converter to DC bus. Moreover, the second voltage source is connected directly to DC bus and there is also a resistive load

connected to the main bus. This microgrid consists of at least four states and one input ( $u$ ) which is the boost converter duty cycle. The state equations of this grid are as follows:

$$\frac{di_{s1}}{dt} = \frac{1}{L_1} (V_{s1} - uv_C) \quad (3-3)$$

$$\frac{di_1}{dt} = \frac{1}{L_2} (v_C - v_{CL} - R_1 i_1) \quad (3-4)$$

$$\frac{dv_C}{dt} = \frac{1}{C} (ui_{s1} - i_1) \quad (3-5)$$

$$\frac{dv_{CL}}{dt} = \frac{1}{C_L} \left( i_1 + i_{s1} - \left( \frac{v_{CL}}{R_L} \right) \right) \quad (3-6)$$

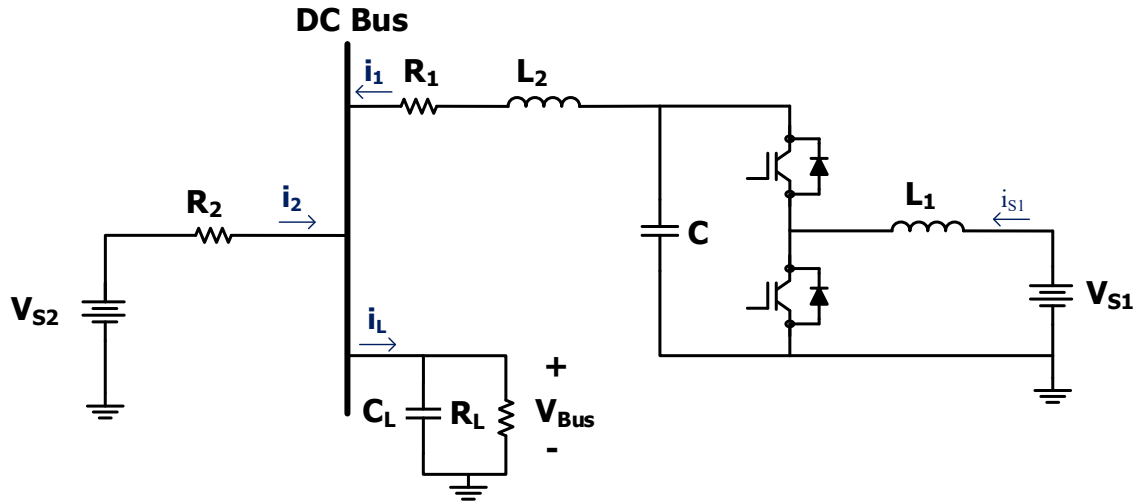


**Figure 3-6:** The basic schematic diagram of the DC microgrid

One of the power supplies is connected to the DC bus through a power electronics converter which makes it controllable. By means of a DC to DC converter, the voltage of source 1 matches the DC bus voltage level and power is transferred from source 1 to the load. In

this system, the voltage of source 2 is fixed but the total power demand of the load is shared between two sources.

### **3.4 FINITE STATE MACHINE IN REAL-TIME APPLICATIONS**

The smart module needs to have a smart control system for identifying the load/source type, configuring DC microgrid, and performing supervisory control of power transfer in the microgrid. This control system first analyzes the voltages and currents of the system and then modifies the switching function of the converter. Moreover, other control commands come from this smart control system. In this project, a Finite State Machine (FSM) as applicable to a real-time system is used as the main controller of the smart module.

A Finite State Machine (FSM) is a mathematical model of computation which could be used for logical control of the reactive systems. A reactive system is one that reacts to external events. The control logic model by means of state machine defines a finite set of states and determines the system transitions flowchart from one state to another, in the presence of certain conditions. In state machine model, the next step depends on current states and its inputs are described as:

$$X(n + 1) = f(X(n), u) \quad (3-7)$$



Where  $X(n)$  is the state at time step  $n$ ,  $X(n + 1)$  is the next step time state and  $u$  represents the inputs. A state is a local data, chart activity, or a combination of both of them. For each computing state process, local variables are updated and the transition is made from one state to another based on the system properties.

The state machine is used in dynamic systems as a complex logic model. It could schedule a set of sequence tasks and supervisory control for switching between different modes of the system. By implementing a state machine in real-time applications, the states of the system that are related to the inputs, are updated in each time step. From one time step to another, state persists. Feedback from the sensors are imported to the model and outputs are changed so that the system meets the desired point of operation.

Stateflow is an environment in MATLAB that functions based on the state machine and flowcharts to simulate the control systems on the basis of decision logic. State diagrams, transition rules, and defining input and output variables are representing the state machine. Designing logic is defining the conditions and constraints to be checked and then performing the planned actions [39].

### **3.5 PID CONTROLLERS**

The state machine provides a control system for the smart module to make a DC microgrid. It also generates the reference values of the desired current and voltage. This system needs

another controller to set the duty cycle of the converter according to the current and voltage feedbacks. A Proportional–Integral–Derivative (PID) controller is one of the most common feedback controllers in industrial applications. The properties of the PID controller can be found in every control theory textbook, but for summarizing key features, the PID algorithm is described as follows:

$$u(t) = K_p e(t) + K_i \int_0^t e(\tau) d\tau + K_d \frac{de(t)}{dt} \quad (3-8)$$

Where  $u$  is the control signal,  $e$  is the control error ( $e = \text{desired value} - \text{measured value}$ ) and  $K_p, K_i, K_d$  are coefficients for the proportional, integral, and derivative terms respectively.

By using only proportional control, the steady state error will decrease with increasing  $K_p$ , but the system's oscillation will increase. By adding an integral section to the controller, the steady state error disappears. However, the system's tendency for oscillation increases. The controller's derivative part is used for setting the damping of system response [40].

As seen in Figure 3-7, two PID controllers are used in the control program of this thesis. First, the PID controller controls the output voltage of the converter to reach the desired value in order to match the output voltage to the DC bus voltage. In the second part, as the voltages are matched and the connection is made, current goes under the control of PID. The implementation of the PID controllers is presented in Figure D-10 in Appendix D. The

PID controller for current should have the initial condition to maintain the voltage at a previous value at the starting point. Meanwhile, the supervisory control of state machine controls the transferred power and the limitations of currents and voltages.

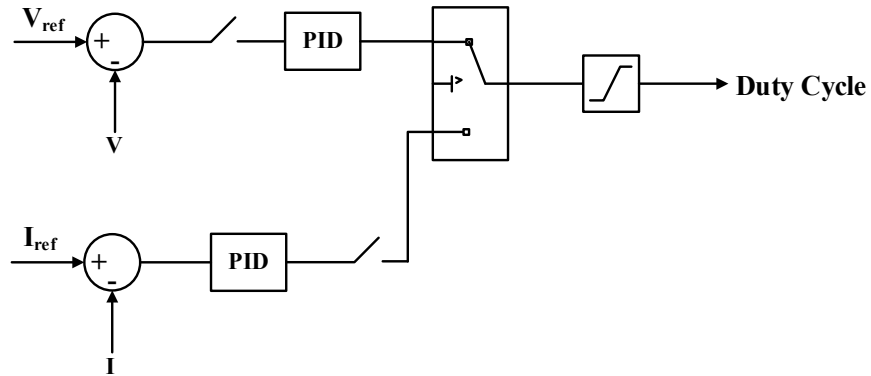


**Figure 3-7:** PID controller scheme implemented for DC microgrid

PID controller is combined with a logic state machine to build the complicated control system for management of this autonomous DC microgrid in this project. The voltage and current references come out of the state machine and compare to actual values from the hardware. The PID controllers generate the duty cycle value of the power electronics driver. By changing the duty cycle, PID attempts to minimize the error and set voltage and current at desired values.

### 3.6 SIMULINK MODEL AND PARAMETER ESTIMATION TOOL

The detailed boost converter model used for simulation during this project is presented in Figure D-1 in Appendix D. By using MATLAB/Simulink R2015a and measured data from the experimental setup, model parameters are modified using Parameter Estimation Tool.

Parameter Estimation is one of the Simulink Design Optimization toolboxes. This toolbox, by comparing the measured data of the experimental setup with simulation outputs, helps to determine which parameter values best fit for this purpose. For this estimation, model parameters, initial conditions, and measured data are used as an input. This toolbox provides some optimization algorithms such as Gradient Descent and Nonlinear Least Squares, and converges according to the desired tolerance and/or number of iterations [41].

By using this tool, the pre-measured inaccurate values of the power board changed a little bit to achieve the most accurate model of the system, not only for a steady state but also for transient behavior. The circuit diagram of the model and the position of parameters are presented in Figure 3-8. Firstly, an initial guess was made according to the experimental measurements and datasheets' information about 9 circuit parameters. The model parameters changed as described in Figure 3-9. All parameters are set to change between 0.1 to 10 times of the actual values. Table A-1 in Appendix A shows exact changes in all of these nine parameters.

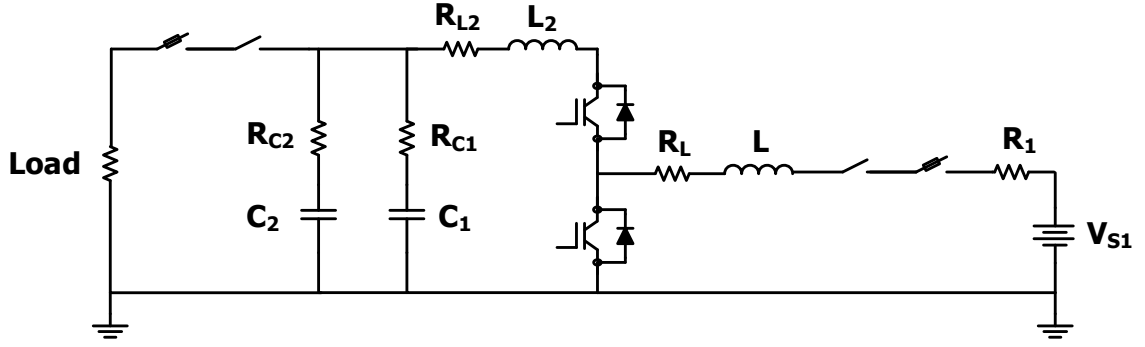


**Figure 3-8:** Simulation model of DC microgrid for parameter estimation

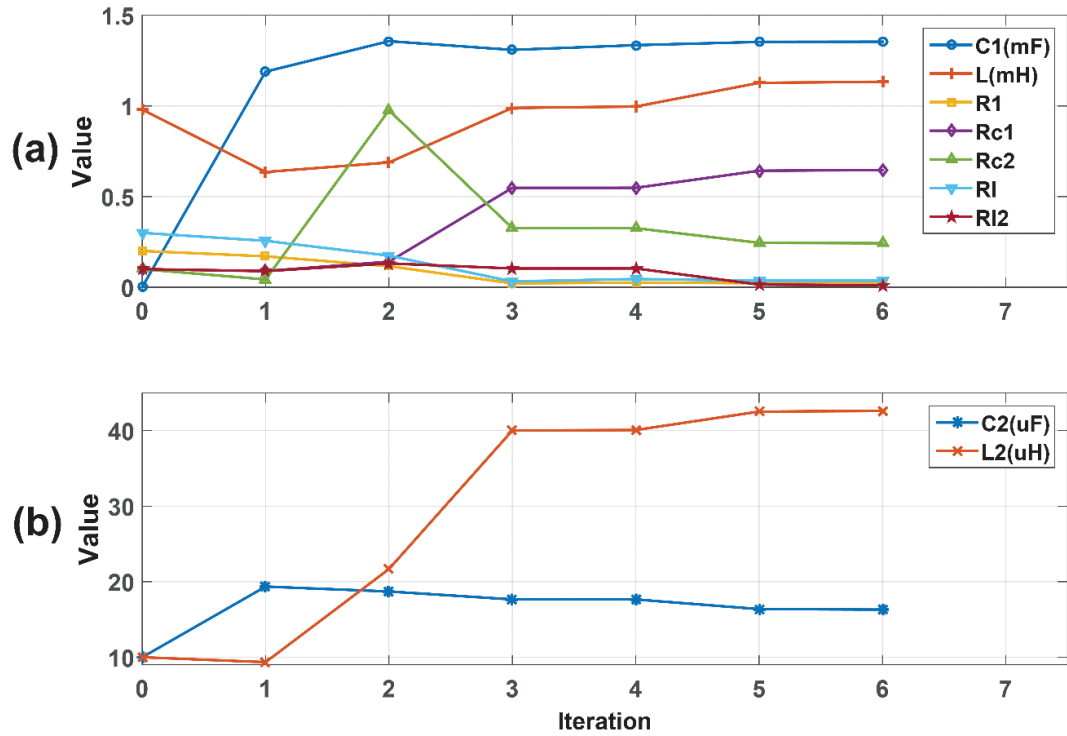


**Figure 3-9:** Estimated parameters in different iterations –

(a)  $C1$ ,  $L$ ,  $R1$ ,  $R_{c1}$ ,  $R_{c2}$ ,  $RI$  and  $RI2$  (b)  $C2$  and  $L2$

As seen in Figure 3-9, all of the model parameters change from initial guess such that the output follows experimental data. In this test, load voltage is considered as an output and

duty ratio of the converter changes from 70% to 50% after 0.5 s. This optimization process stops when the relative sum of squares goes below the desired value of 0.001 in this model.

Table 3-3 shows the measured values of the system parameters and estimated parameters at final iteration. For some of the values such as capacitors and inductance (C1, C2, L), measured values are considered as an initial guess. The capacitors series resistances of the C1 and C2 are  $0.129\ \Omega$  at 100 Hz and  $0.013\ \Omega$  at 10 kHz, respectively. Additionally, cables which connect these elements to the other parts of the board have some resistances.

**Table 3-3:** Changing simulation model parameters from initial guess to final value by Parameter Estimation Tool and measured parameters

	<b>C1 (mF)</b>	<b>C2 (<math>\mu</math>F)</b>	<b>L (mH)</b>	<b>L2 (mH)</b>	<b>R1 (<math>\Omega</math>)</b>	<b>Rc1 (<math>\Omega</math>)</b>	<b>Rc2 (<math>\Omega</math>)</b>	<b>Rl (<math>\Omega</math>)</b>	<b>Rl2 (<math>\Omega</math>)</b>
<b>Measured</b>	0.918	10.88	0.988	0.014	0.014	0.3	0.08	0.01	0.007
<b>Iteration 6</b>	1.354	16.312	1.133	0.042	0.0222	0.6462	0.2424	0.0361	0.0102

The Parameter Estimation Tool changes the system parameters so the output of the model tracks measured data. The whole system has more than 9 parameters, but in this estimation process, 9 of them are estimated. Therefore, the response of the whole system changes only based on these parameters. Because of this, the estimated parameters change from measured values to new ones. Moreover, there are some small parameters that are not considered in the simulation model but exist in the experimental setup.

The experimental data and simulated output are compared by using Parameter Estimation Tool in Figure 3-10. As seen, except the variation of experimental data which is influenced by the sensor noise, the simulation result is as expected.

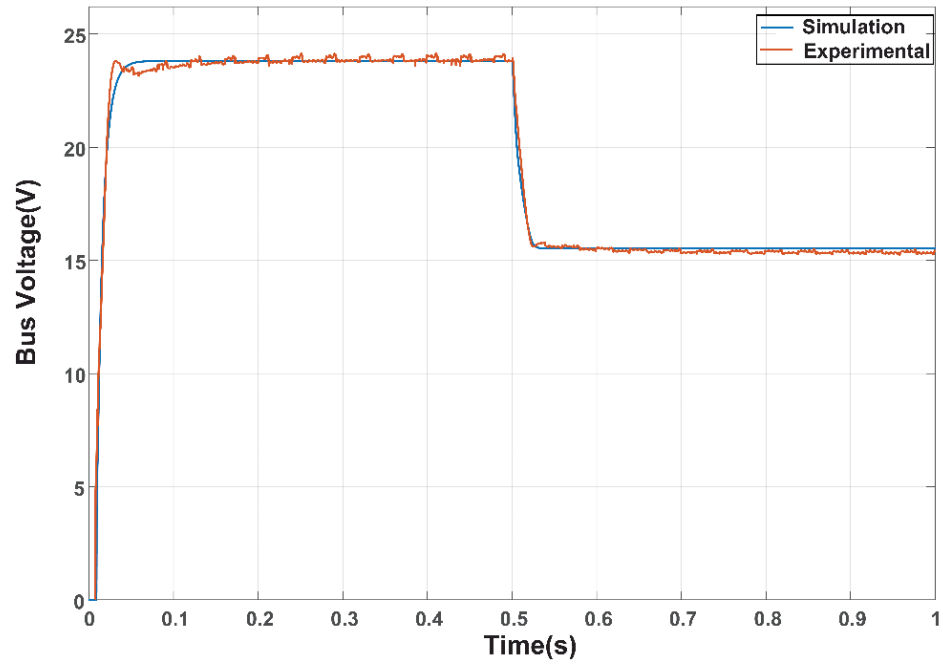


**Figure 3-10:** Measured data and simulation output by parameter estimation

## **CHAPTER 4**

### **EXPERIMENTAL APPARATUS AND RESULTS**

This chapter presents the details of the experimental setup to configure the smart autonomous DC microgrid. After introducing the identification circuit, the other hardware and software parts of this project are presented. The apparatus configuration and controlling programs are tested under different experimental situations. DC microgrid connects battery, DC SMPS, loads, and is used for load sharing and transferring power.

#### **4.1 IMPLEMENTING IDENTIFICATION METHOD**

The load identification system consists of three resistors as a load, which are connected to the electrical component for analyzing terminal voltage, shown in Figure 4-1. The power range of the resistors is 10 W to draw out the least possible current from sources. The switches between resistors could change the total resistance value according to the input voltage range. The combined resistance could be 220  $\Omega$ , 68.75  $\Omega$ , and 52.3  $\Omega$ . For this



study, resistors are connected in parallel so the identification method can be used for the range of 0 V to 30 V.

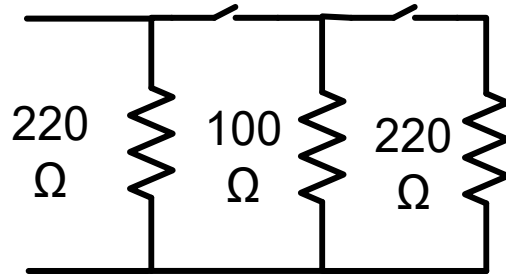


**Figure 4-1:** Experimental setup for identification method

#### 4.1.1 BATTERY STATE OF CHARGE (SOC) TABLE

As seen in Figure 3-5 (a), as the current increases, the voltage drop in the exponential region would be more significant especially during the first 50 seconds. By considering a resistor as a load while the battery discharges, as the discharge current rate goes up, the resistor should be smaller in size and larger in power rating. As a result, the power loss of identification circuit becomes larger. This identification system requires a trade-off between power losses, time of identification, and resistor size.

Table 4-1 shows voltage drop values, SOC variations, and power losses of the 12 V battery with both 53 Ω and 5.3 Ω resistors as a load. In the same period of time, the voltage and SOC of the battery for smaller resistor decrease more. This table is implemented in the

identification system as a reference for determining the battery SOC. Based on the SOC, the control system determines whether to charge the battery or connect to the DC grid.

**Table 4-1:** Battery voltages for different initial state of charge with two different resistors (White: 53  $\Omega$ , Gray: 5.3  $\Omega$ ) for a 2 minute period

Starting Point Voltage (V)	Middle Point Voltage (V)	Ending Point Voltage (V)	Initial SOC of Battery (%)	Final SOC of Battery (%)	Power Losses (W)
13.0338	12.8240	12.6832	100	99.9193	3.205282
13.0007	12.2941	12.2736		99.2219	31.89023
12.3019	12.2942	12.2940	80	79.9227	2.85541
12.2707	12.1938	12.1917		79.2327	28.40945
12.1928	12.1825	12.1822	60	59.9234	2.804988
12.1618	12.0596	12.0560		59.2410	27.90743
11.9746	11.9592	11.9585	40	39.9248	2.705491
11.9442	11.7917	11.7839		39.2577	26.91772
11.3199	11.2897	11.2872	20	19.9290	2.417738
11.2911	10.9930	10.9643		19.3073	24.05452

The detailed model of the battery is used for testing the aforementioned identification system. The simulation results of the battery's terminal voltage across parallel resistors are presented in Figure 4-2. The similarity between all the battery voltages for different SOC values is the decreasing exponential trend of the voltage in the first 30 seconds period of discharging time.

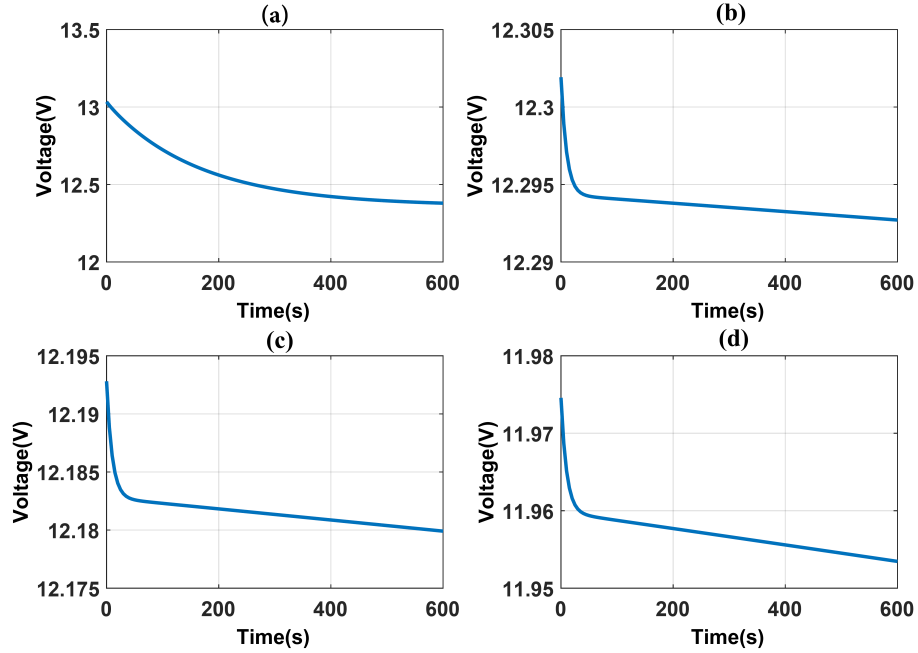


**Figure 4-2:** Simulation results of battery voltage in (a) 100% initial SOC (b) 80% initial SOC (c) 60% initial SOC and (d) 40% initial SOC with constant 53  $\Omega$  resistive load

#### 4.1.2 LOADS AND SOURCES IN THE CONFIGURED GRID

The load and source types for this part of the experiment are presented in Table 4-2. The sources of electrical energy could be a charged battery or a DC power supply connected to the national grid. By means of these sources, the resistive loads, LED, DC motor and uncharged batteries receive electrical energy. The other types of loads and sources which could also be tested and analyzed are presented in Table 4-3.

**Table 4-2:** Loads and sources for validating identification results

<b>Loads</b>	<b>Sources</b>
DC motor LED light Resistive load Uncharged battery	Battery DC source

**Table 4-3:** Possible loads and sources in DC microgrids

<b>Sources and Storage Devices</b>	<b>Loads</b>
Wind Turbines Microturbine Supercapacitors Photovoltaic (PV) Vanadium Redox Battery (VRB) Flywheel Compressed air system	Factory loads Data centers Charging stations for Electrical Vehicle (EV)

As all of the sources and loads connect to each other to form the DC grid, the type of sources and loads in terms of AC or DC determines the type of power converter which connects them to the grid (AC-DC or DC-DC). Moreover, the voltage level of sources settles the control scheme for voltage matching. Meanwhile, the supervisory control takes responsibility of load power sharing according to available sources, current limitation, etc.

### **4.1.3 DECISION TREE FOR DC MICROGRID WITH DC POWER SUPPLY AND BATTERY**

The load identification method used for this project could differentiate a battery from a DC source, and also loads from sources. As seen in Figure 4-3, after connecting the load identification circuit to a black box, by measuring the voltage for less than a minute the type of electrical equipment such as load, DC source and battery could be identified. After that, the battery SOC is determined which in turn establishes the battery role as a source (charged) or a load (uncharged). If the DC power supply is present in the microgrid and the DC source capacity is not full, the power would be transferred to the load and the battery will be charged. At all times, the energizing source priority for the load would be the DC power source and then the battery in the absence of electricity from the grid.

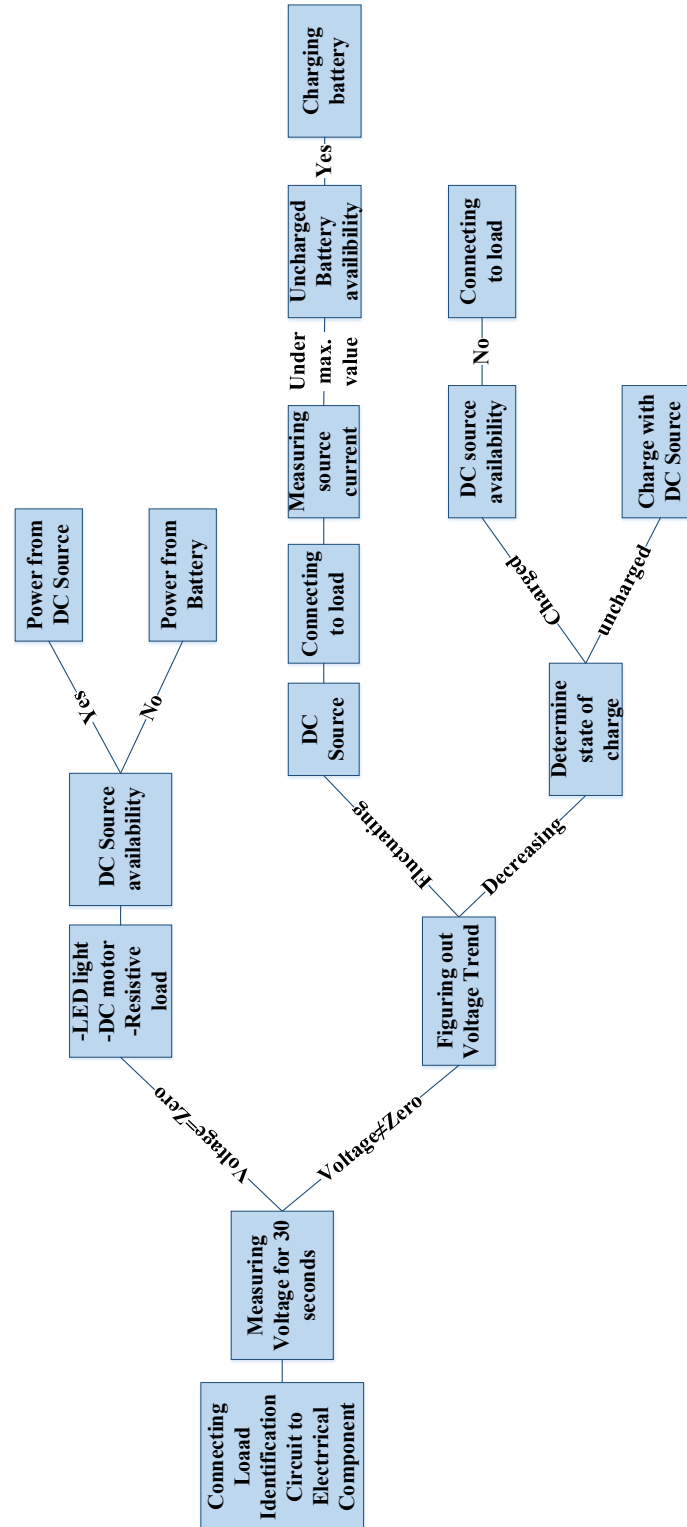


**Figure 4-3:** Simulation Decision Tree of identification method and transferring power

#### 4.1.4 EXPERIMENTAL DISCHARGE BEHAVIOR OF THE 12 V BATTERY

The 12 V battery as specified in Table 3-2 was connected to a 53  $\Omega$  resistive load which was used as the identification circuit. As shown in Figure 4-4, the battery was fully charged in (a) and the same procedure was repeated for this battery at different charge levels from 95% to 6%. The experimental results show the exponential trend of discharging the battery in the first 20 seconds of connecting the load. The final voltage value of the discharging process is used for deriving the SOC percentage of the battery.

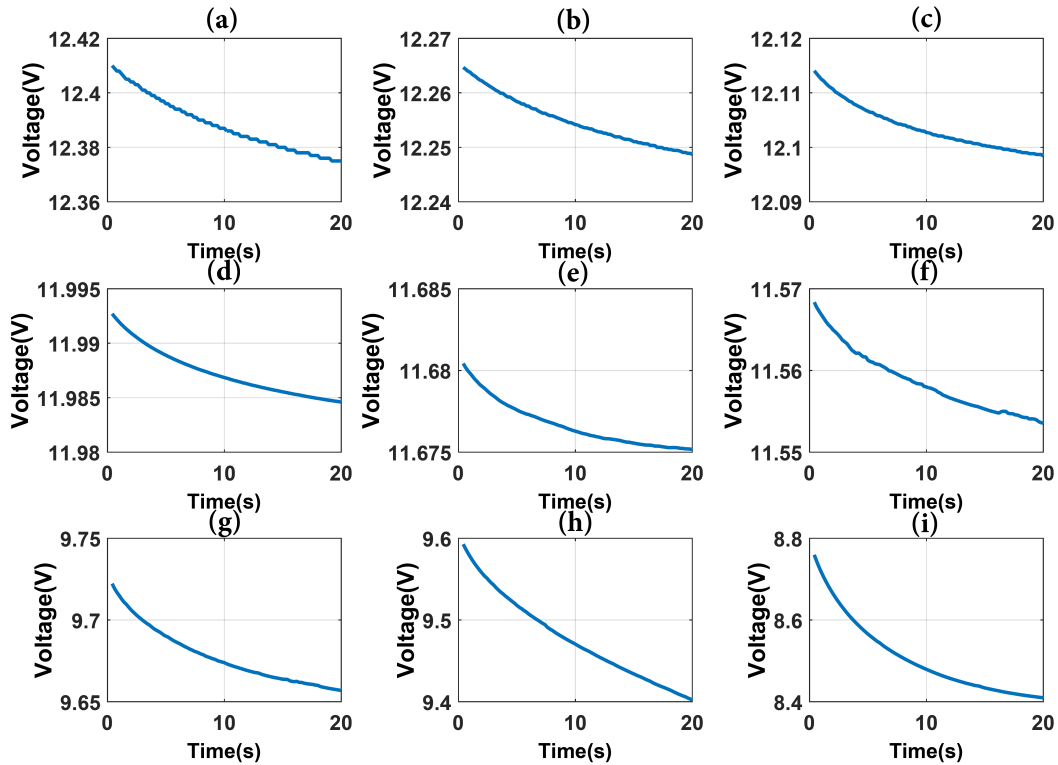


**Figure 4-4:** Experimental discharge rate of 12V battery from –  
(a) 95% SOC to (i) 6% initial SOC

## **4.2 EMBEDDED COMPUTER CONTROL SYSTEM**

As discussed in 3.4, the control system of the proposed module in the DC microgrid works for real-time application. Real-time computation needs an embedded system to perform pre-defined tasks based on the feedback from the hardware. The PC/104 is one of the embedded computer standards which is usually used in places that require a small, rugged, and cost-effective form of PC. The PC/104 were introduced in 1987 and developed for designers who worked on embedded systems and needed to control and monitor real-world inputs and outputs of the system. In 1992, PC/104 Consortium was established and made PC/104 an internationally recognized standard.

The most noticeable advantage of PC/104-Plus is its modular and stackable form factor. PC/104 design and connectors make it possible to have modules stacked like building blocks. This reduces the size and cost of the embedded computer.

In PC/104 series, instead of using a backplane, modules pair together via stackable ISA, PCI, and PCIe bus connectors. The stackable connectors make a compact and rugged PC system. Digital I/O, analog I/O, CPU, DataCom, and communication modules from different manufacturers stack over each other to make compact, highly powerful computer and data acquisition systems.



The main applications of PC/104 are military, energy, and transportation. Moreover, this powerful and rugged PC is also found in mining, traffic monitoring, heavy lifting, and industrial control [42, 43].

In this experimental apparatus, 3-stacked PC/104-Plus is used as shown in Figure 4-5. The modules are CPU, timer/counter and analog I/O. The CPU module is the top module in Figure 4-5, and some of its specifications are provided in Table 4-4.



**Figure 4-5:** PC/104-Plus with three stacked modules - CPU (top), Timer/Counter (middle), and Analog I/O (bottom)

**Table 4-4:** PC/104-Plus CPU module specifications

<b>CPU</b>	AMD LX800
<b>Front-Side Bus (FSB) Speed</b>	133 MHz
<b>Performance</b>	500 MHz
<b>Memory Type</b>	SODIMM200–2.5 V/DDR
<b>Memory Speed max.</b>	DDR 400
<b>Max. Memory</b>	1,024 MB
<b>Buses</b>	ISA and PCI

The second module is the Mesa 4I22 Timer/Counter module. This module is responsible for making Pulse Width Modulation (PWM) signals for converter's switches. This is a 10 MHz, 9-channel, universal counter-timer card. Moreover, this module can be used in many other applications such as event counting, frequency counting, interrupt timers, etc. The main features of this module are presented in Table 4-5 [44].

**Table 4-5:** Mesa 4I22 Timer/Counter module features

Nine 16 bit 10 / 25 MHz counters
24 bit parallel I/O port
10 / 25 MHz trimmable timebase
Socketed PIO and counters

The lowest module in aforementioned PC/104-Plus is analog I/O module. In Table 4-6, the main specifications of the analog and digital I/O ports are presented. By implementing this module, the PC is able to handle the outputs of voltage and current sensors as analog input.

**Table 4-6:** Diamond-MM-32DX-AT analog and digital I/O specifications [45]

<b>Analog Inputs</b>	<b>Digital I/O</b>
32 input channels, 16-bit resolution	24 bi-directional lines using integrated 8255-type circuit
Programmable gain, range, and polarity on inputs	Buffered I/O for enhanced current drive
250,000 samples per second maximum sampling rate	User-configurable pull-up / pull-down resistors
Auto-calibration of all input ranges under software control	Handshaking controls enable external latching of data as well as interrupt operation

Table 4-7 shows the resolution of the analog input of this module. Moreover, this module has digital I/O header which is appropriate for creating commands for electrical devices such as switches (digital output) and input commands from the operator (digital input). The User Datagram Protocol (UDP) along with serial communication was used to pass PWM signals to the PCB for switching and voltage and current feedbacks to the PC/104-Plus.

**Table 4-7:** Diamond-MM-32DX-AT 16-Bit Analog I/O

<b>Polarity</b>	<b>Range</b>	<b>Full-Scale Range</b>	<b>Resolution</b>
Bipolar	5 V	$\pm 5$ V	153 $\mu$ V

### 4.3 SIMULINK REAL-TIME

A real-time embedded controller by means of MATLAB/Simulink Real-Time is used as the main monitoring and supervisory controlling system of the microgrid. Simulink Real-Time lets a designer create Simulink models for real-time applications and runs models on the target computer which is connected to the physical system. For setting up Simulink Real-Time, a single PCI bus target computer, network target boot method, and a C compiler are needed.

After that, the IP-based connection between developer and target computer is established. Then, target settings are configured and boot method configuration for target PC is set up through Simulink Real-Time Explorer.

By using MathWorks embedded code generation, instead of writing a control system which would take thousands of lines of code by hand, the generated code of the Simulink model is built on the target PC. Some other main features of Simulink Real-Time are [46]:

- Automatic generation of the real-time application from Simulink model to target PC.
- Driver blocks in Simulink library to access analog and digital I/O ports.
- Simulink Real-Time Explorer to access target computer for management of real-time applications.

MATLAB/Simulink is used to build the model-based design of the control system on the target PC. Through this process of building the whole control system on the PC/104-Plus,

target PC is converted to the main control system that no longer needs a further connection to the host PC. However, keeping a connection between the host and target PCs brings the possibility of a real-time control system.

## 4.4 SMART MODULE CONFIGURATION

The DC microgrid schematic diagram is presented in Figure 4-6. For making such a DC microgrid, the smart module is needed to identify load/source type and then transfer power from source to load. Firstly, the power electronics converter comes to mind. As seen in Figure 4-7, the PCB board is installed to function as a converter. A 6-switch converter is presented in Figure 4-8. It has three pairs of IGBTs with parallel free-wheeling diodes and common ground and DC bus. For making the DC microgrid, the DC and U phases of the converter are used as a boost converter with a series inductor and parallel DC capacitors.

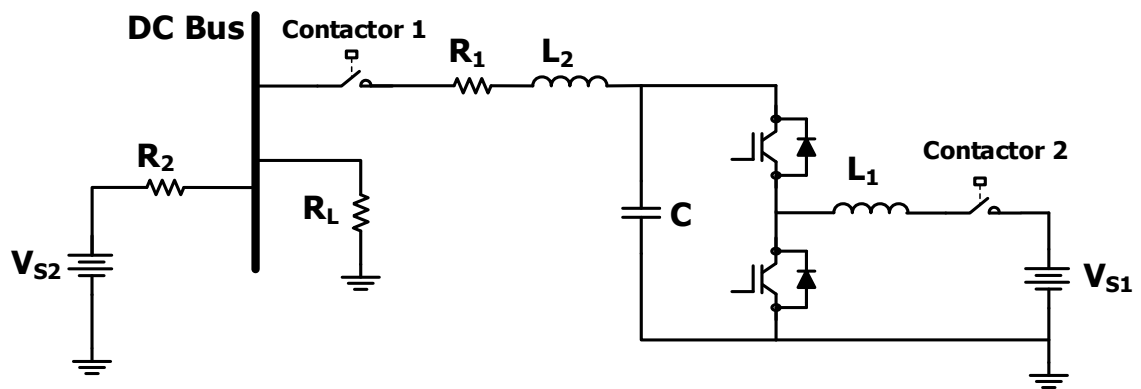


**Figure 4-6:** DC Microgrid configuration

The contactors are used not only for making the connection between source and converter but also to connect/disconnect the smart module to the DC bus. The contactors' driver

provides sufficient current and voltage to turn the contactors on or off. The voltage sensors are used for voltage measurement for both identification and control systems. The voltage sensors are installed on both sides of the contactors to measure the voltage.

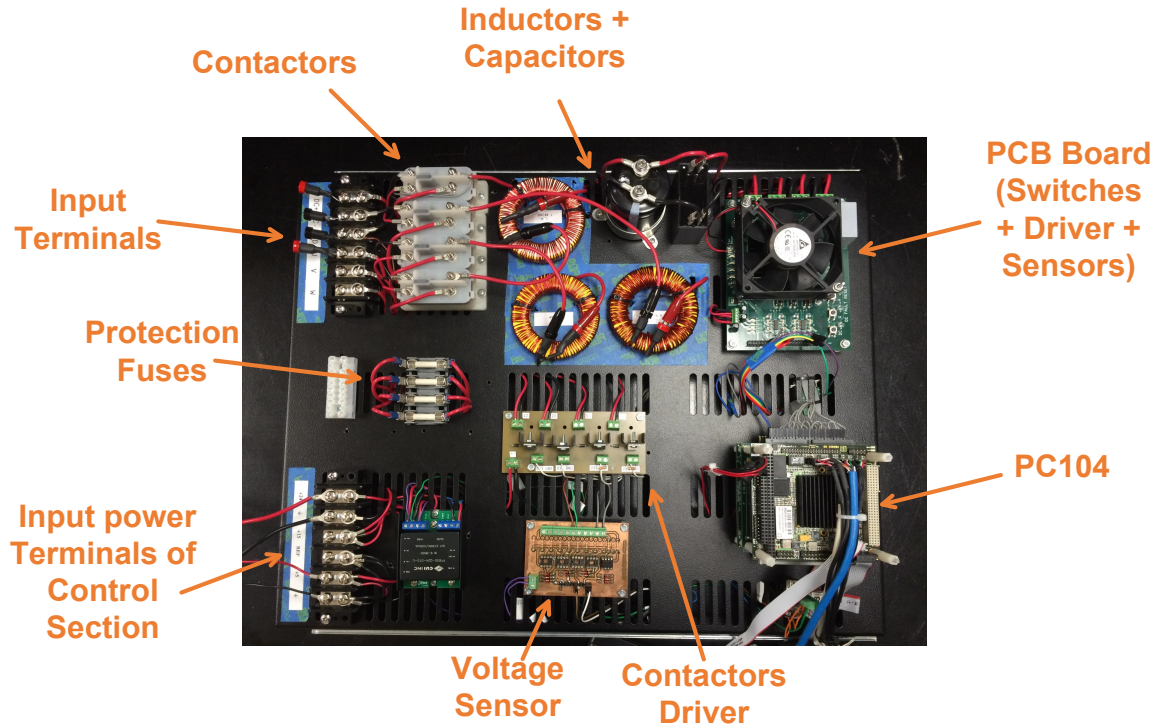


**Figure 4-7:** Experimental setup of smart module configuration

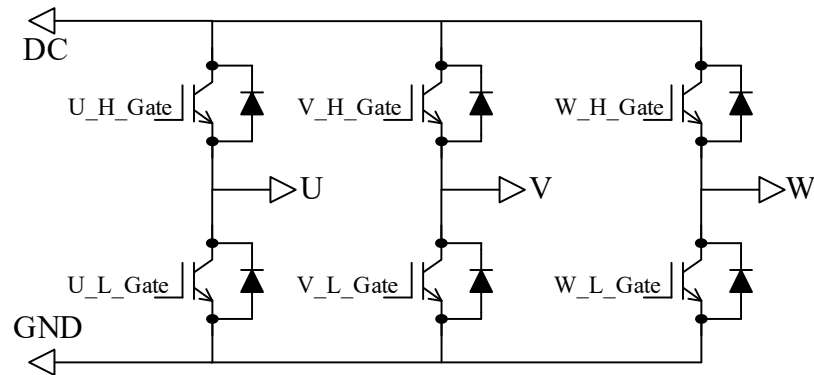


**Figure 4-8:** Converter's switches (IGBT) configuration "Adapted from [47]"

As discussed in 4.3, the Simulink Real-Time runs Simulink models on target computer hardware which is connected to the physical system. The target PC/104-Plus is also connected wirelessly to the host PC in order to run real-time applications. As shown in Figure 4-9, the PC/104-Plus creates not only PWM switching functions for the switches on the power stage PCB but also generates commands for contactors that connect the source and the load to the DC bus.

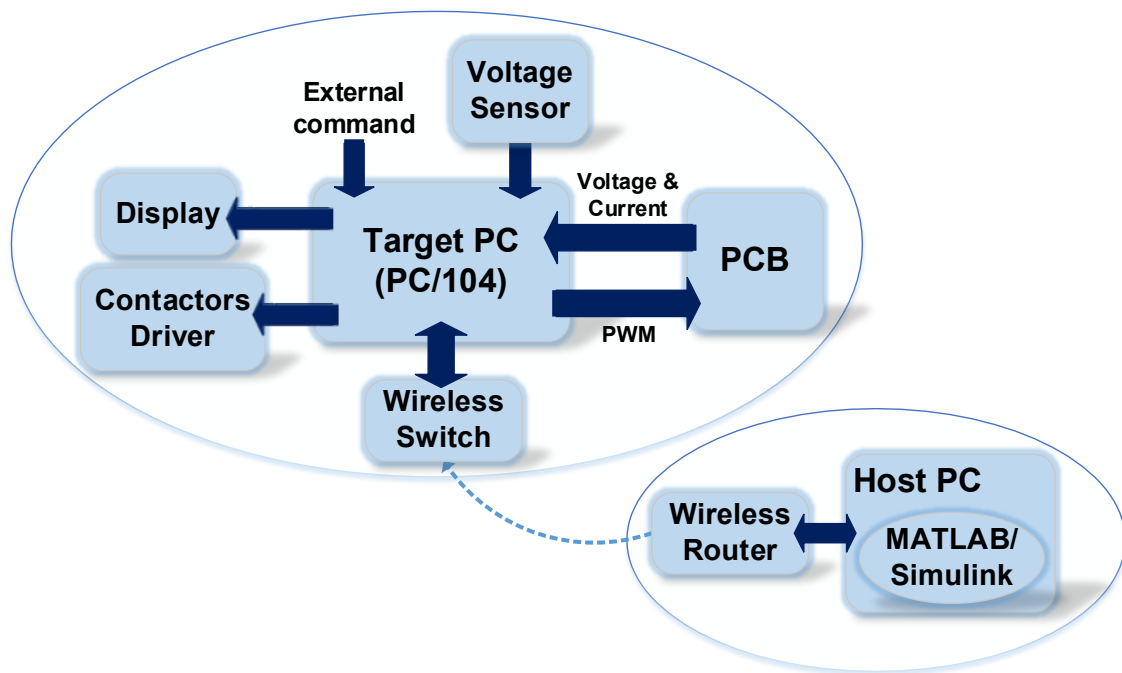


**Figure 4-9:** PC/104-Plus connections with Host PC and other parts of power electronics board

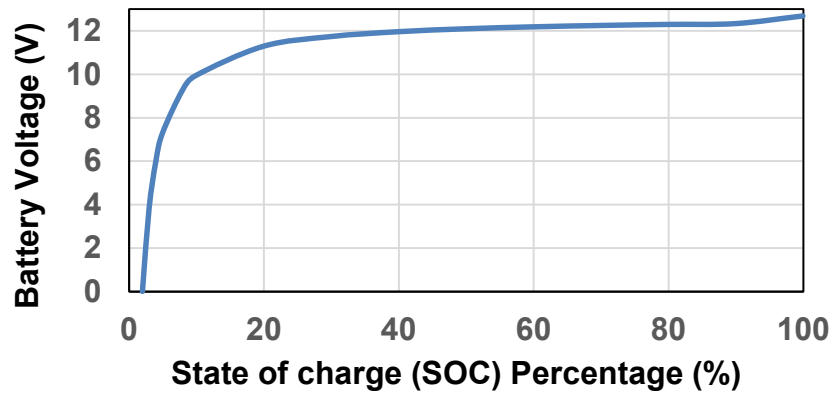
## 4.5 EXPERIMENTAL RESULTS

The first step of configuring the DC grid is to identify the type of electrical component. The parallel resistors are connected to one of the phase terminals of the converter (DC or U). As voltage sensors are installed on both sides of the contactors, the contactors are open and voltage sensor measures the voltage of the source/load which is connected to the identification circuit.

The identification loop samples mean voltage value of the voltage sensors which is calculated in time period intervals of 3 seconds. The sampling time is 0.001 seconds and at the end of 30 seconds, the voltage trend is derived. As discussed before in 3.2, the battery voltage decreases exponentially at the beginning of the discharge process while the DC power supply voltage does not reveal the same trend.

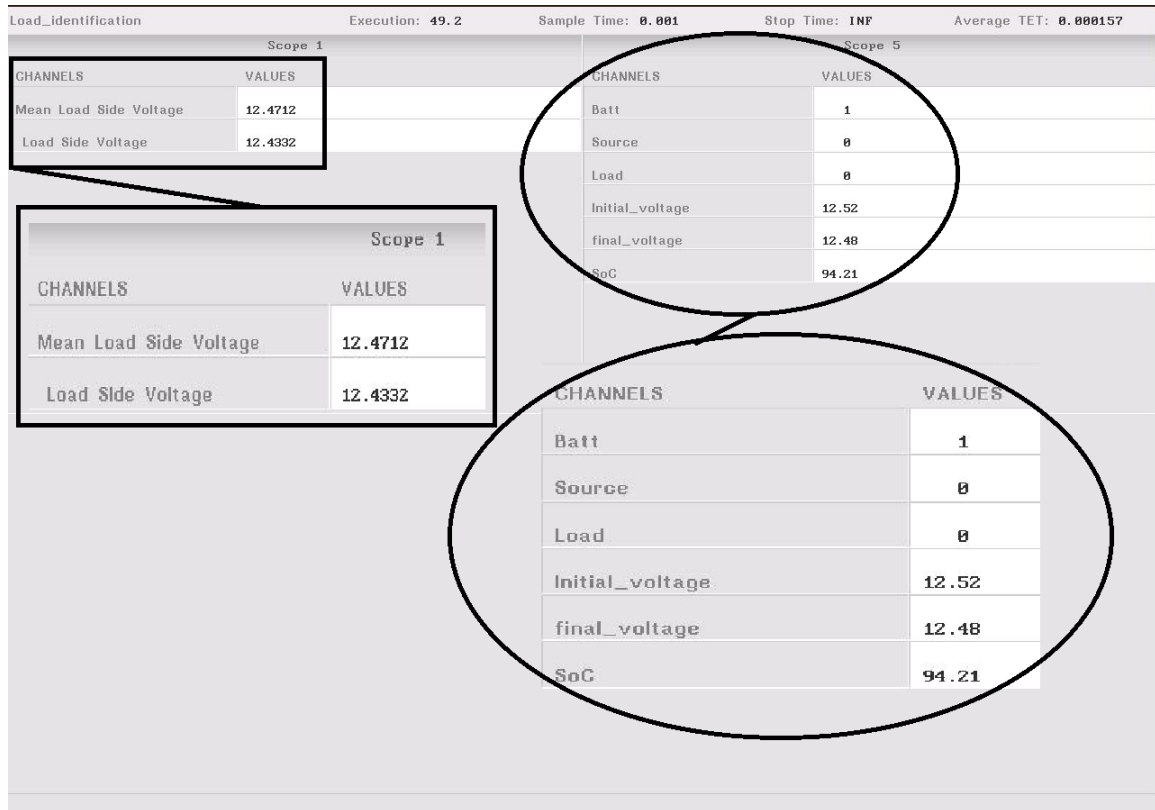
As for the battery, the state of charge is important, hence the lookup table implemented in the main model shows the percentage of battery charge. The state of charge values are extracted from the accurate Simulink model which block parameters in MATLAB/Simulink are presented in Table D-1 in Appendix D. In Table B-2 in Appendix B, all data points that are used to figure out the SOC value of the battery while discharging are presented. Figure 4-10, which is based on the simulation results of the tested battery, shows the battery voltage dropping drastically for values below the 20% state of charge.





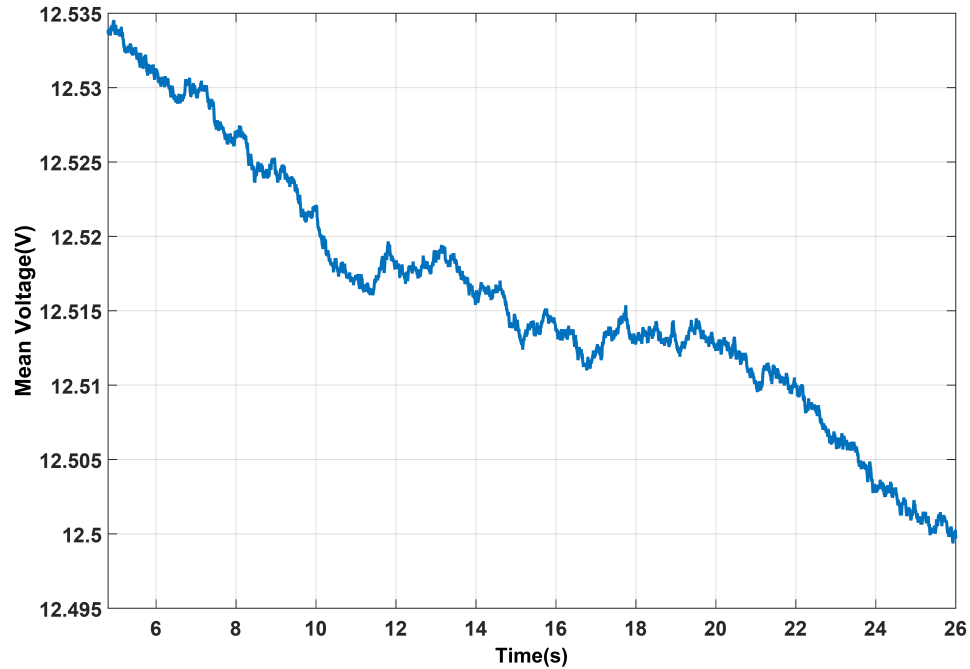
**Figure 4-10:** Simulation result of the tested battery voltage versus state of charge (SOC) percentage

Figure 4-11 shows the target screen while the battery is connected to the identification circuit. This screenshot demonstrates the result of the load/source identification system, and the decision is made by changing the allocated amount from 0 to 1 for each of the electrical components. Moreover, it shows the battery SOC (%) and terminal voltage. For example, in Figure 4-11, it shows the electrical device is identified as a battery (Batt = 1) and the state of charge of the battery is 94.21%. Moreover, the last measurement of the source voltage is 12.48 V.



**Figure 4-11:** Simulink Real-Time target screen of connecting battery to identification circuit

The mean voltage of the battery terminals while connected to the identification resistors is presented in Figure 4-12. These samples have been pulled out from the voltage sensor of the Power Electronics Board (PEB). The voltage decreased as expected from 12.53 V to 12.5 V during first 20 seconds of connection to the load.



**Figure 4-12:** Battery voltage mean values during the first 20 seconds of connecting the identification resistors

The same procedure is repeated for the DC power supply. The Xantrex DC power supply is used as the constant 15 V source of energy. The control system detected the DC power supply as the source (Source = 1) and measured the voltage for 30 seconds. Figure 4-13, the capture screen of the PC/104-Plus display, shows the control system decision after the power supply connection.

Load_identification		Execution: 37.5	Sample
Scope 1			
CHANNELS		VALUES	
Mean Load Side Voltage		15.0467	
Load Side Voltage		15.1722	
Scope 5			
CHANNELS		VALUES	
Batt		0	
Source		1	
Load		0	
Initial_voltage		15.04	
final_voltage		15.05	
SoC		0.00	

**Figure 4-13:** Simulink Real-Time target screen of connecting DC power supply to the identification circuit

The measured voltage of the source over 53  $\Omega$  resistor is presented in Figure 4-14. The mean value of the aforementioned voltage changes irregularly between initial and final voltage values. Meanwhile, the voltage level does not decrease in the same way as the battery trend.

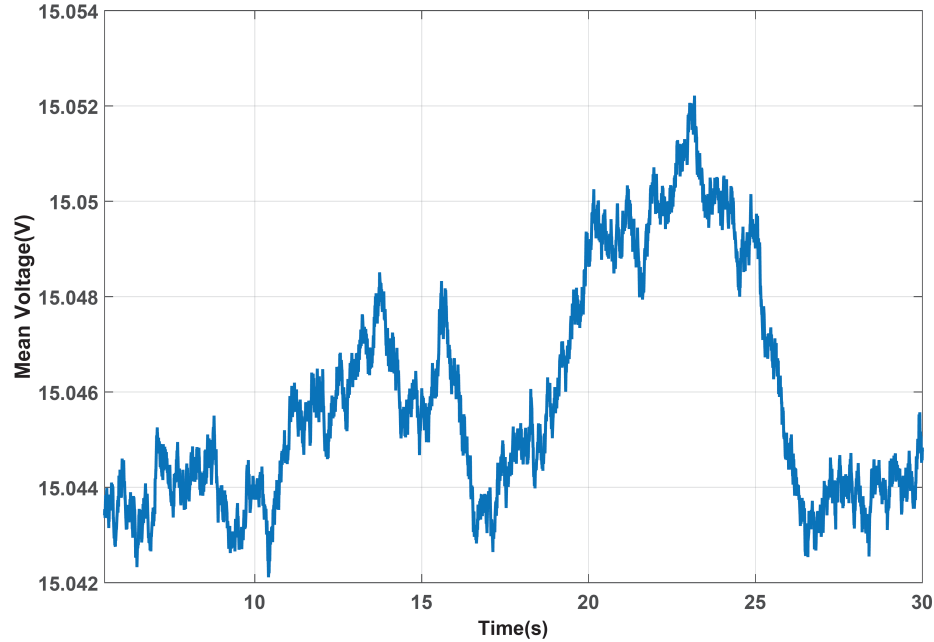


**Figure 4-14:** DC power source voltage mean values during the first 30 seconds of connecting the identification resistors

## 4.6 TRANSFERRING POWER FROM SOURCE TO LOAD

The presented board and control system has the ability to control the current, voltage, and power. The power board wiring connections and more details are presented in Appendix C. The output voltage is regulated at the desired value while the current, power, and the total time of transferring power are under control. This means that the system could control the behavior of the DC microgrid according to the voltage, current, power, and time separately or in combination. To demonstrate this feature, two load types (LED light and DC motor) are paralleled as a connected load to the DC bus. The DC power supply voltage

is boosted to a specific voltage level. This configuration is indicated in Figure 4-15. There are other specifications about the LED and DC motor detailed in [48] and [49].

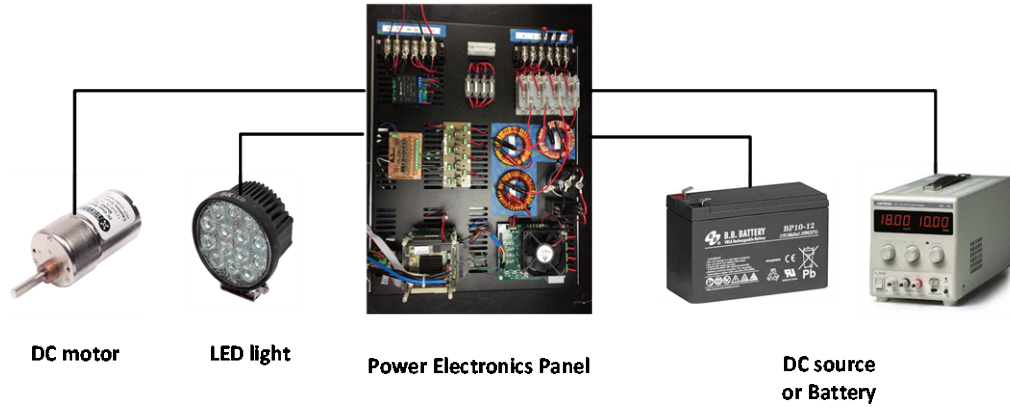


**Figure 4-15:** Transferring power from DC source to LED and DC motor

In this example, the goal is providing an output voltage between 12 V to 20 V and transferring a specific amount of energy to the loads. The bus voltage, source current, and load side current are presented in Figure 4-16. The series inductance of source is 1.946 mH and DC bus capacitor magnitude is 470  $\mu$ F. The DC source could be 12 V battery or DC power supply at 12 V.

For this kind of power transfer process, first the voltage goes to the minimum voltage level of the boost converter with 10% duty cycle and then increases till current reaches the maximum planned current. There is also the possibility of limiting transferring energy, according to other constraints such as source current, current-carrying capacity of the conductors, etc.

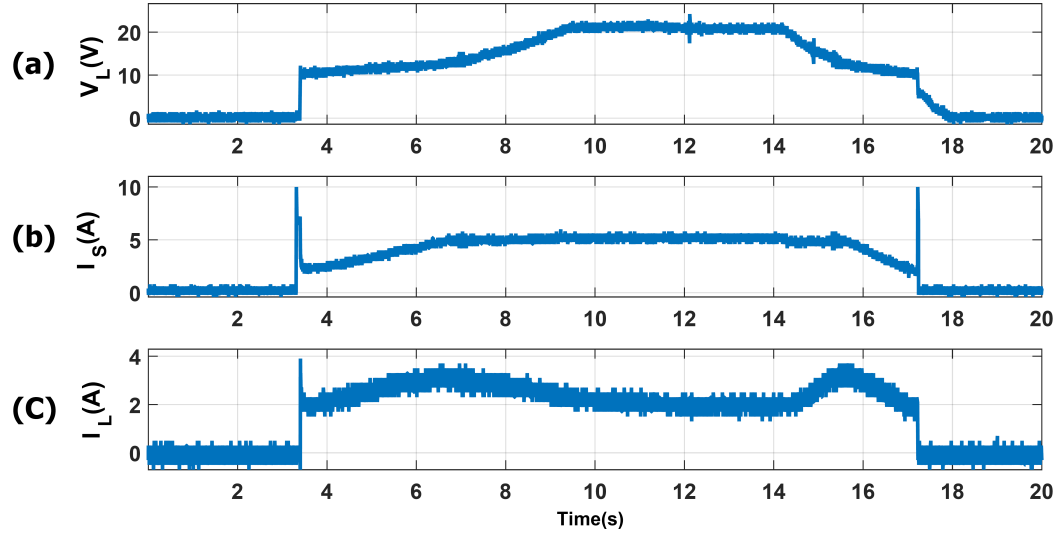


**Figure 4-16:** Experimental results of DC Microgrid with LED and DC Motor as load  
(a) DC Bus voltage (b) Current injected from source to panel (c) Load current

## 4.7 LOAD SHARING

The common configuration of a simple DC microgrid is shown in Figure 3-6. In this model, 2 power supplies are responsible for providing energy for load and controlling DC bus voltage. One of the sources is connected through power electronics device to DC bus, making it a controllable source. On the other hand, source 2 is connected directly to the DC bus. Each of them could be DC voltage source or battery or any other types of DC voltage source. The experimental parameters of the DC grid setup are listed in Table 4-8.

First, a main controlling system without PI controller is tested. Figure 4-17 shows the DC bus voltage, current from DC source 1 (battery) converter to the load and current flows from the other source (DC power supply) to the DC bus.

**Table 4-8:** Load sharing experimental variables

Series Inductance	DC Capacitors	Load Resistance	Source 1 (Battery)	Source 2 (DC supply)	Transferred Energy
1.946 mH	1000 $\mu$ F Electric Double Layer+ 10 $\mu$ F Film capacitor	11.49 $\Omega$	12 V	20 V	400 J

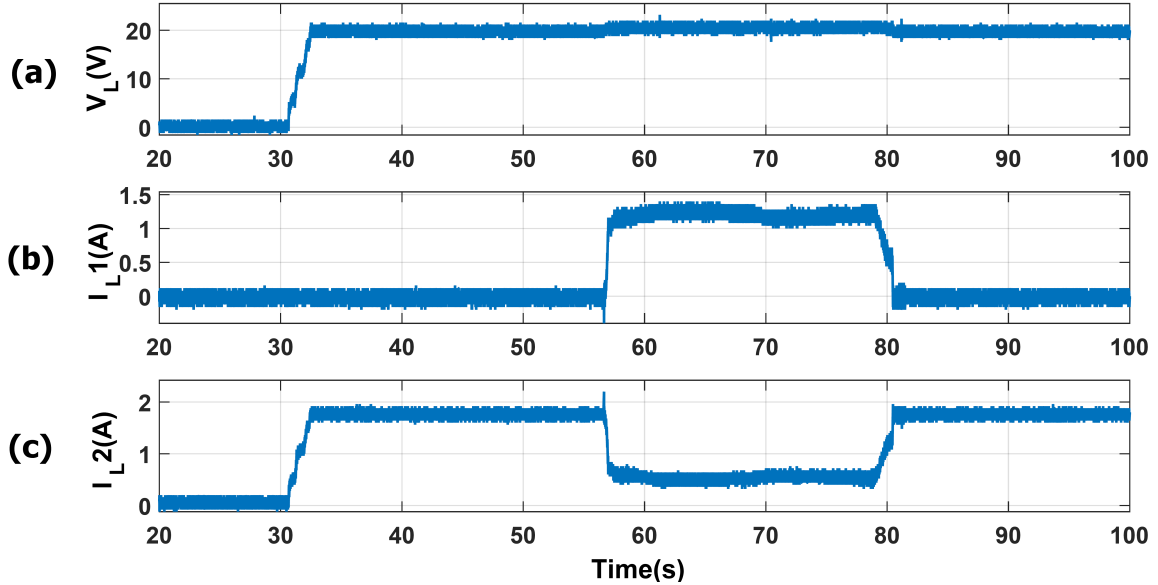


**Figure 4-17:** Experimental outputs for load sharing (a) DC Bus voltage (b) Load current from source 1 (c) Load current from source 2



In the previous load transferring energy, duty cycle comes from the state machine with control over voltage, current, and power. First, the output voltage of the source number 1 through the power electronics converter is changed to the DC bus voltage value. At this point, the voltage values on both sides of the contactor 1 are the same. Then, the source 1 could be connected to the DC grid safely. By considering the current limits of both the source and power electronics device, the duty cycle is changed. After that, the power is transferred to the load (DC bus) at the maximum level. When the power reaches to around 90% of desired power, the duty cycle changes to decrease injected current from source 1 to the DC bus to zero. Then, the source disconnects from the grid. The flowchart of this control scheme is presented in Figure 4-18. State machine diagram and real-time Simulink models with more details are provided in Figure D-7 through Figure D-9 in Appendix D.

Another example of load sharing is about the system with batteries as sources. The parameters of this system are provided in Table 4-9. The battery voltage of one side is less than 13 V while the other side is more than 23 V. The importance of matching voltage at DC bus point comes to attention in this case.

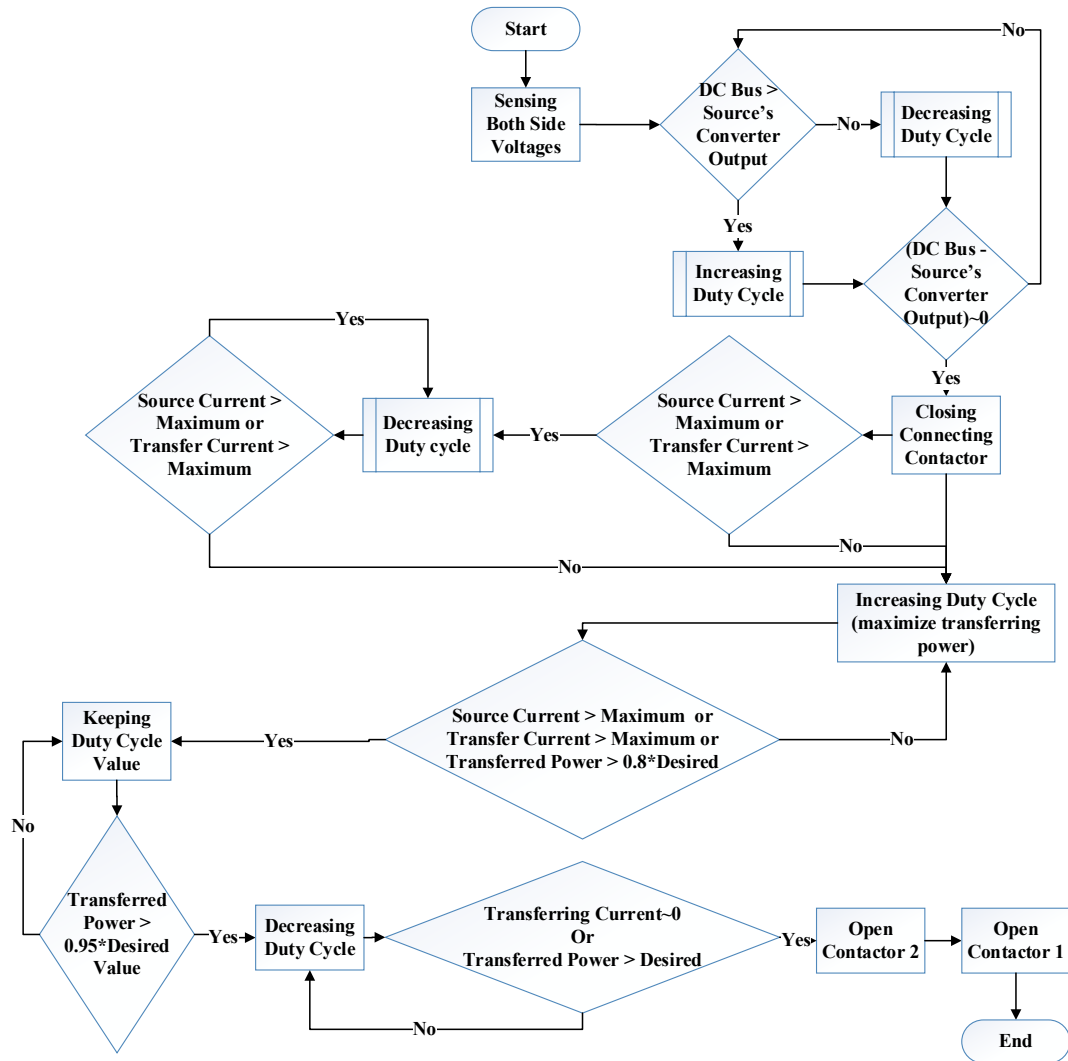


**Figure 4-18:** Flowchart diagram of the DC Microgrid control scheme

**Table 4-9:** Experimental Parameters of load sharing between batteries

<b>Series Inductance</b>	<b>DC Capacitors</b>	<b>Load Resistance</b>	<b>Source 1 (Battery)</b>	<b>Source 2 (Battery)</b>	<b>Transferred Energy</b>
1.946 mH	1000 $\mu$ F Electric Double Layer+ 10 $\mu$ F Film capacitor	5.8 $\Omega$	12.8 V	23.3 V	400 J

As seen from the results in Figure 4-19, Source 2 is responsible for energizing the resistive load. Then, source 1 comes to connect to DC Grid with 4 constraints:

- Matching voltage level same as the DC bus voltage.
- Maximum transfer current below 2 A.
- Maximum current from source 1 below 4 A.
- Transferring 400 J energy from source 1 to the load.

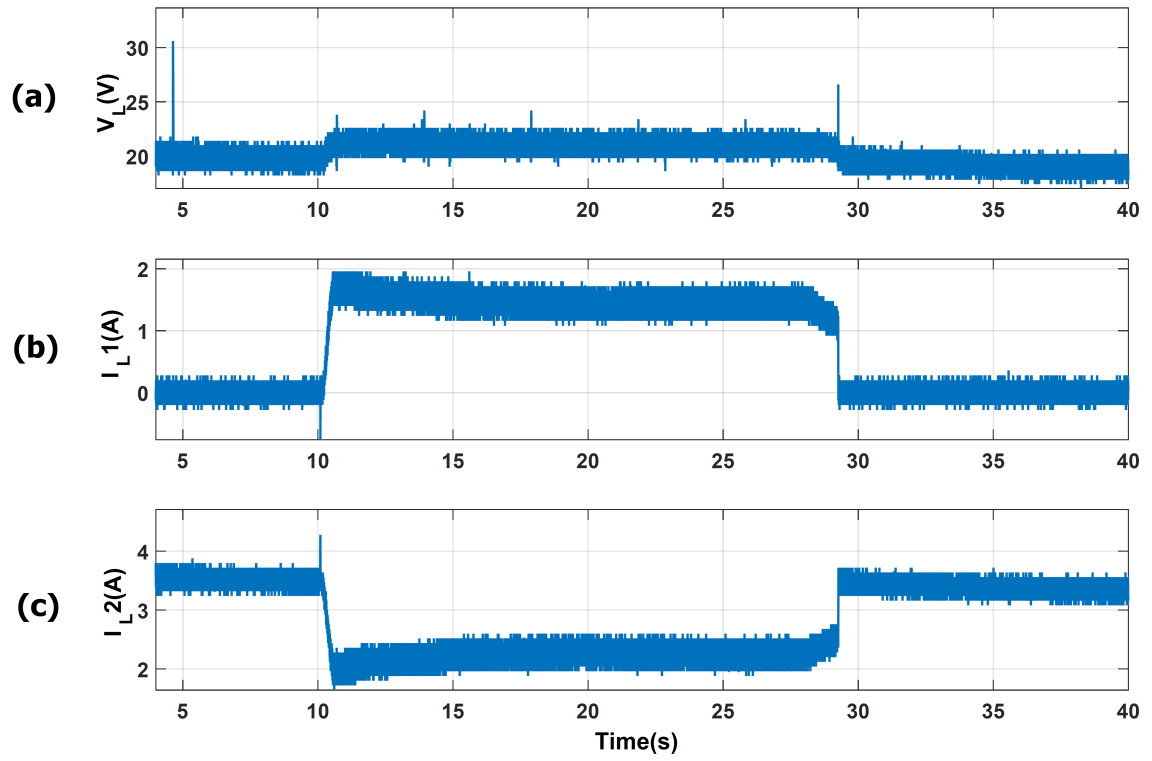


**Figure 4-19:** Experimental outputs for load sharing between two batteries (a) DC Bus voltage (b) Load current from source 1 (c) Load current from source 2

# **CHAPTER 5**

## **CONCLUSIONS**

### **5.1 SUMMARY OF ACCOMPLISHMENTS**

This research has demonstrated the load/source identification method for DC microgrid applications. The self-configurable type of microgrid can employ this identification method to set up grids from existing unknown power sources and loads. As a source type, this system can identify batteries from DC power supplies by considering the exponential voltage trend of the discharge characteristics. Moreover, the battery state of charge (SOC) is determined by using the battery's terminal voltage. After load/source identification, the DC grid is configured according to the availability of source types. This identification method along with control of the microgrid is validated by the experimental setup of the DC microgrid. The 4 main constraints of the system - current, bus voltage, transferred energy, and time, with the help of the state machine and real-time application, control the microgrid efficiently and confidently.

## **5.2 RECOMMENDATIONS FOR FUTURE WORK**

This thesis presents a method for identification of source types in the DC microgrid. This method may also be useful in AC and Hybrid AC/DC microgrids.

For future work, it would be beneficial to extending the identification method to recognize active and passive loads from each other. In this case, an external power source could be mounted beside identification circuits to inject currents toward loads and analyze the output voltages and currents.

Furthermore, developing identification decision methods for other types of sources such as PV, wind farms, and diesel generators may also be useful in microgrid configurations. This could be useful when all of the DG sources are connected to each other.

## REFERENCES

- [1] T. S. Ustun, C. Ozansoy, and A. Zayegh, "Recent developments in microgrids and example cases around the world—A review," *Renewable and Sustainable Energy Reviews*, vol. 15, pp. 4030-4041, 10// 2011.
- [2] M. A. Hassan and M. A. Abido, "Real time implementation and optimal design of autonomous microgrids," *Electric Power Systems Research*, vol. 109, pp. 118-127, 4// 2014.
- [3] Y. H. Lin, M. S. Tsai, and C. S. Chen, "Applications of fuzzy classification with fuzzy c-means clustering and optimization strategies for load identification in NILM systems," in *IEEE International Conference on Fuzzy Systems, FUZZ 2011*, pp. 859-866.
- [4] S. N. Backhaus, G. W. Swift, S. Chatzivasileiadis, W. Tschudi, S. Glover, M. Starke, *et al.*, "DC Microgrids Scoping Study. Estimate of Technical and Economic Benefits," LA-UR--15-22097 United States, 2015.
- [5] L. Mariam, M. Basu, and M. F. Conlon, "A Review of Existing Microgrid Architectures," *Journal of Engineering*, vol. 2013, p. 8, 2013.
- [6] R. Faulkner. (2013). *AC vs. DC Powerlines and the Electrical Grid*. Available: <http://theenergycollective.com/rogerrethinker/204396/ac-versus-dc-powerlines>

- [7] B. R. Blasi, "DC Microgrids: review and applications," Dept. Arch. Eng. and Cons. Sc., College of Engineering, Kansas State University, M.S. report 2013.
- [8] J. M. Guerrero, J. C. Vasquez, J. Matas, M. Castilla, and L. G. d. Vicuna, "Control Strategy for Flexible Microgrid Based on Parallel Line-Interactive UPS Systems," *IEEE Trans. Ind. Electron.*, vol. 56, pp. 726-736, 2009.
- [9] J. M. Guerrero, P. C. Loh, T. L. Lee, and M. Chandorkar, "Advanced Control Architectures for Intelligent Microgrids-Part II: Power Quality, Energy Storage, and AC/DC Microgrids," *IEEE Trans. Ind. Electron.*, vol. 60, pp. 1263-1270, 2013.
- [10] R. H. Lasseter and P. Paigi, "Microgrid: a conceptual solution," in *IEEE 35th Annual Power Electronics Specialists Conference, PESC*, 2004, pp. 4285-4290 Vol.6.
- [11] D. Infield and F. Li, "Integrating micro-generation into distribution systems -a review of recent research," in *Power and Energy Society General Meeting - Conversion and Delivery of Electrical Energy in the 21st Century*, 2008, pp. 1-4.
- [12] A. Sannino, G. Postiglione, and M. H. J. Bollen, "Feasibility of a DC network for commercial facilities," *IEEE Trans. Ind. Applicat.*, vol. 39, pp. 1499-1507, 2003.
- [13] J. M. Guerrero, J. C. Vasquez, J. Matas, L. G. d. Vicuna, and M. Castilla, "Hierarchical Control of Droop-Controlled AC and DC Microgrids&-A General Approach Toward Standardization," *IEEE Trans. Ind. Electron.*, vol. 58, pp. 158-172, 2011.



- [14] N. Calamero, Y. Beck, and D. Shmilovitz, "Defining the Unique Signatures of Loads Using the Currents' Physical Components Theory and Z-Transform," *IEEE Trans. Ind. Informat.*, vol. 11, pp. 155-165, 2015.
- [15] H. H. Chang, L. S. Lin, N. Chen, and W. J. Lee, "Particle Swarm Optimization based non-intrusive demand monitoring and load identification in smart meters," in *IEEE Industry Applications Society Annual Meeting , IAS*, 2012, pp. 1-8.
- [16] Ó. Jiménez, Ó. Lucía, L. A. Barragán, D. Navarro, J. I. Artigas, and I. Urriza, "FPGA-Based Test-Bench for Resonant Inverter Load Characterization," *IEEE Trans. Ind. Informat.* , vol. 9, pp. 1645-1654, 2013.
- [17] R. A. S. Fernandes, I. N. d. Silva, and M. Oleskovicz, "Load Profile Identification Interface for Consumer Online Monitoring Purposes in Smart Grids," *IEEE Trans. Ind. Informat.*, vol. 9, pp. 1507-1517, 2013.
- [18] V. P. Sakthivel, R. Bhuvaneswari, and S. Subramanian, "Non-intrusive efficiency estimation method for energy auditing and management of in-service induction motor using bacterial foraging algorithm," *IET Electric Power Applicat.*, vol. 4, pp. 579-590, 2010.
- [19] H. Eristi and Y. Demir, "Automatic classification of power quality events and disturbances using wavelet transform and support vector machines," *IET Generation, Transmission & Distribution*, vol. 6, pp. 968-976, 2012.
- [20] M. Biswal and P. K. Dash, "Measurement and Classification of Simultaneous Power Signal Patterns With an S-Transform Variant and Fuzzy Decision Tree," *IEEE Trans. Ind. Informat.*, vol. 9, pp. 1819-1827, 2013.

- [21] R. Alcaraz, E. J. Bueno, S. Cobrecas, F. J. Rodriguez, F. Espinosa, and S. Muyulema, "Power System Voltage Harmonic Identification Using Kalman Filter," in *12th International Power Electronics and Motion Control Conference, EPE-PEMC 2006*, pp. 1283-1288.
- [22] F. Kupzog, T. Zia, and A. A. Zaidi, "Automatic electric load identification in self-configuring microgrids," in *AFRICON*, 2009, pp. 1-5.
- [23] N. W. A. Lidula and A. D. Rajapakse, "Microgrids research: A review of experimental microgrids and test systems," *Renewable and Sustainable Energy Reviews*, vol. 15, pp. 186-202, 1// 2011.
- [24] R. H. Lasseter, "MicroGrids," in *IEEE Power Engineering Society Winter Meeting*, 2002, pp. 305-308 vol.1.
- [25] N. R. a. J. Spitaels, "A Quantitative Comparison of High Efficiency AC vs DC Power Distribution for Data Centers," *Schneider Electric White Paper*, vol. 127, p. 20, 2012.
- [26] L. Shiguo, Y. Zhihong, L. Ray-Lee, and F. C. Lee, "A classification and evaluation of paralleling methods for power supply modules," in *IEEE 30th Annual Power Electronics Specialists Conference, PESC 1999*, pp. 901-908 vol.2.
- [27] L. Xu and D. Chen, "Control and Operation of a DC Microgrid With Variable Generation and Energy Storage," *IEEE Tran. Power Del.*, vol. 26, pp. 2513-2522, 2011.

- [28] P. Karlsson and J. Svenson, "Voltage Control and Load Sharing in DC Distribution Systems," presented at the European Conference on Power Electronics and Applications, EPE Toulouse, 2003.
- [29] T. M. Haileselassie and K. Uhlen, "Precise control of power flow in multiterminal VSC-HVDCs using DC voltage droop control," in *IEEE Power and Energy Society General Meeting*, 2012, pp. 1-9.
- [30] R. A. F. Ferreira, P. G. Barbosa, H. A. C. Braga, and A. A. Ferreira, "Analysis of non-linear adaptive voltage droop control method applied to a grid connected DC microgrid," in *Brazilian Power Electronics Conference, COBEP*, 2013, pp. 1067-1074.
- [31] Z. M. Salameh, M. A. Casacca, and W. A. Lynch, "A mathematical model for lead-acid batteries," *IEEE Trans. Energy Convers.*, vol. 7, pp. 93-98, 1992.
- [32] M. A. Casacca and Z. M. Salameh, "Determination of lead-acid battery capacity via mathematical modeling techniques," *IEEE Trans. Energy Convers.*, vol. 7, pp. 442-446, 1992.
- [33] M. Ceraolo, "New dynamical models of lead-acid batteries," *IEEE Trans. Power Syst.*, vol. 15, pp. 1184-1190, 2000.
- [34] M. Dürr, A. Cruden, S. Gair, and J. R. McDonald, "Dynamic model of a lead acid battery for use in a domestic fuel cell system," *Journal of Power Sources*, vol. 161, pp. 1400-1411, 10/27/ 2006.
- [35] C. M. Shepherd, "Design of Primary and Secondary Cells," *J. Electrochem. Soc.*, vol. 112, p. 657, 1965.

- [36] O. Tremblay, L. A. Dessaint, and A. I. Dekkiche, "A Generic Battery Model for the Dynamic Simulation of Hybrid Electric Vehicles," in *IEEE Vehicle Power and Propulsion Conference, VPPC*, 2007, pp. 284-289.
- [37] S. Zoroofi, "Modeling and Simulation of Vehicular Power Systems," M.S. thesis, Dept. Ener. and Env., Chalmers University of Technology, Goteborg, Sweden, 2008.
- [38] Mathworks. (2016). *Implement generic battery model*. Available:  
[http://www.mathworks.com/help/physmod/sps/powersys/ref/battery.html?s\\_tid=gn\\_loc\\_drop](http://www.mathworks.com/help/physmod/sps/powersys/ref/battery.html?s_tid=gn_loc_drop)
- [39] MathWorks. (2016). *Stateflow*. Available:  
<http://www.mathworks.com/products/stateflow/features.html#key-features>
- [40] K. J. Åström and R. M. Murray, *Feedback Systems: An Introduction for Scientists and Engineers*, v2.11b ed. vol. 2012. 41 William Street, Princeton, New Jersey: PRINCETON UNIVERSITY PRESS, 2012.
- [41] MathWorks. (2016). *Simulink Design Optimization*. Available:  
<http://www.mathworks.com/products/sl-design-optimization/features.html#estimation-of-model-parameters-from-test-data>
- [42] R. E. T. Inc. (2016). *What is PC/104? Rugged, Compact, Stackable and Modular*. Available: <http://www.rtd.com/PC104/>
- [43] PC104.com. (2014). *What is PC104?* Available: <http://pc104.com/what-is-pc104/>
- [44] M. Electronics, "4I22 TIMER / COUNTER," M. Electronics, Ed., ed. Richmond, CA 94806-1950: Mesa Electronics, 2016.

- [45] D. S. Corporation, "DMM-32DX-AT User Manual," vol. Rev A.03, D. S. Corporation, Ed., ed. Mountain View, CA 94043: Diamond Systems Corporation, 2011, p. 56.
- [46] MathWorks. (2016). *Simulink Real-Time*. Available: <http://www.mathworks.com/products/simulink-real-time/features.html>
- [47] R. D. Smith, "DC Microgrid stabilization through fuzzy control of interleaved, heterogeneous storage elements," M.S., Dept. Elec. and Com. Eng., Michigan Technological University, Houghton, 2014.
- [48] K. LED, 2016. Available: <http://www.6kled.com/LED-342-p/led-342.htm>
- [49] TETRIX, 2016. Available: <https://c10645061.ssl.cf2.rackcdn.com/resources/tetrix/152motor739530>
- [50] T. Eichhorn, "Boost Converter Efficiency Through Accurate Calculations," *Power Electronics Technology, National Semiconductor, Grass Valley, Calif*, p. 6, 2008 2008.
- [51] D. Gravoc and M. Purschel, "IGBT Power Losses Calculation Using the Data-Sheet Parameters," *Infineon Tech. AG, Neubiberg, Germany*, p. 17, 2009 2009.

# APPENDIX A

## PARAMETER ESTIMATION RESULTS

**Table A-1:** Simulation model's parameters changing in iterations

It.	C1 (mF)	C2 ( $\mu$ F)	L (mH)	L2 ( $\mu$ H)	R1 ( $\Omega$ )	Rc1 ( $\Omega$ )	Rc2 ( $\Omega$ )	RI ( $\Omega$ )	RI2 ( $\Omega$ )
0	1	10	0.98	10	0.2	0.1	0.1	0.3	0.1
1	1.189	19.355	0.63549	9.352	0.17057	0.089218	0.042683	0.25597	0.088763
2	1.357	18.705	0.68814	21.674	0.1162	0.14069	0.97588	0.17422	0.13136
3	1.309	17.658	0.98893	40.013	0.02123	0.54804	0.32598	0.031849	0.10344
4	1.335	17.651	0.99638	40.08	0.02572	0.54813	0.32598	0.04531	0.1038
5	1.353	16.375	1.1272	42.518	0.02233	0.64253	0.24494	0.036278	0.01469
6	1.354	16.312	1.1331	42.61	0.02228	0.64623	0.24247	0.036126	0.010234

# APPENDIX B

## BATTERY DISCHARGE PROCESS

**Table B-1:** Simulation Results of Battery voltages for initial SOC from 10 % to 100 % with two different resistors (White: 53  $\Omega$ , Gray: 5.3  $\Omega$ ) for 2 minutes period

Starting Point Voltage (V)	Middle Point Voltage (V)	Ending Point Voltage (V)	Initial SOC of Battery (%)	Final SOC of Battery (%)	Power Losses (W)
13.0338	12.8240	12.6832	100	99.9193	3.205282
13.0007	12.2941	12.2736		99.2219	31.89023
12.3383	12.3314	12.3313	90	89.9224	2.872333
12.3070	12.2386	12.2369		89.2299	28.57778
12.3019	12.2942	12.2940	80	79.9227	2.85541
12.2707	12.1938	12.1917		79.2327	28.40945
12.2552	12.2463	12.2461	70	69.9230	2.833772
12.2240	12.1363	12.1335		69.2363	28.19362
12.1928	12.1825	12.1822	60	59.9234	2.804988
12.1618	12.0596	12.0560		59.2410	27.90743
12.1055	12.0932	12.0927	50	49.9239	2.764965
12.0748	11.9524	11.9472		49.2477	27.50958
11.9746	11.9592	11.9585	40	39.9248	2.705491
11.9442	11.7917	11.7839		39.2577	26.91772
11.7563	11.7360	11.7348	30	29.9262	2.607747
11.7265	11.5246	11.5111		29.2742	25.94543
11.3199	11.2897	11.2872	20	19.9290	2.417738
11.2911	10.9930	10.9643		19.3073	24.05452
10.0105	9.9531	9.9445	10	9.9374	1.890757
9.9851	9.4259	9.3300		9.4049	18.81174

# APPENDIX C

## SMART MODULE LAYOUT

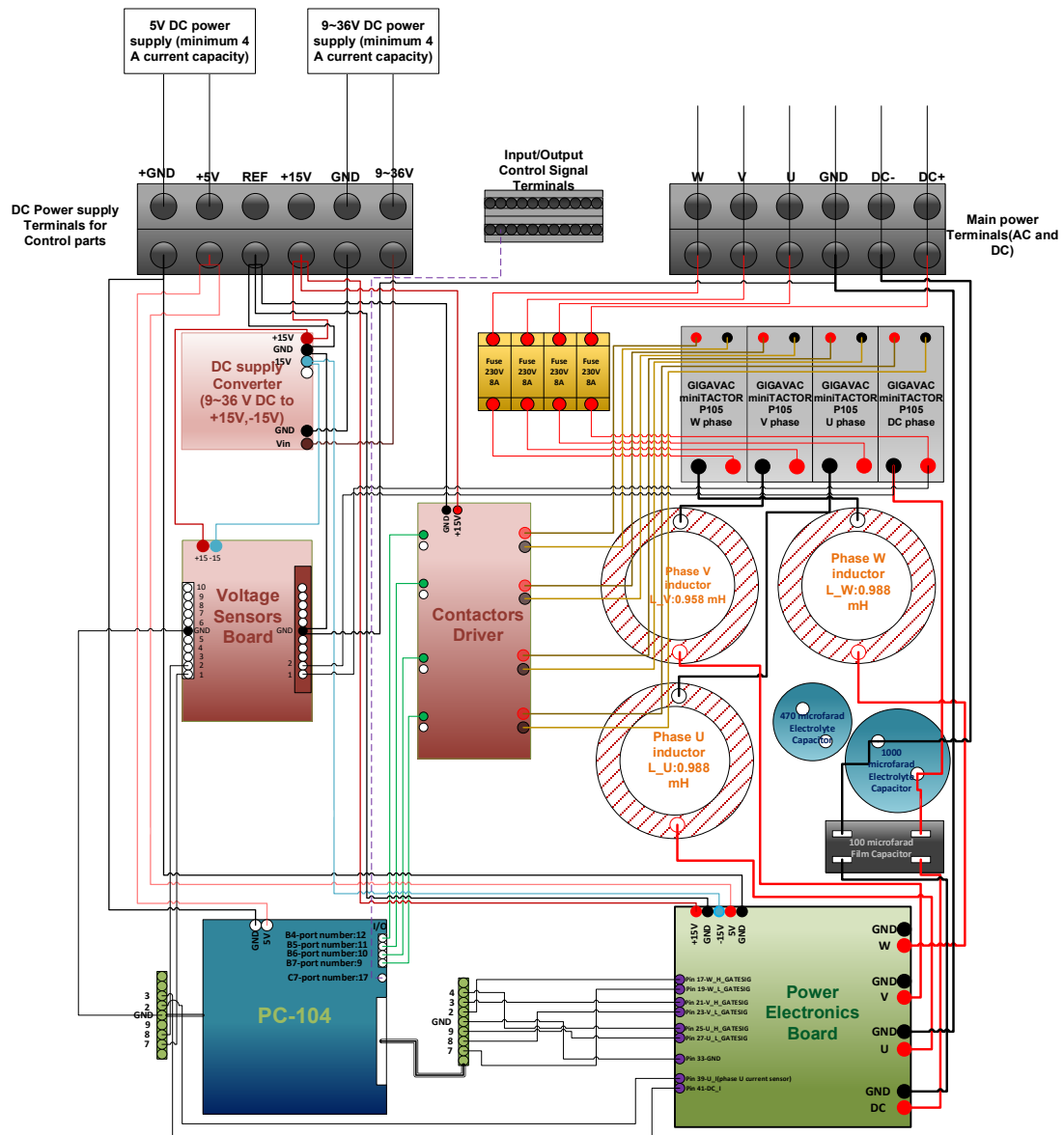
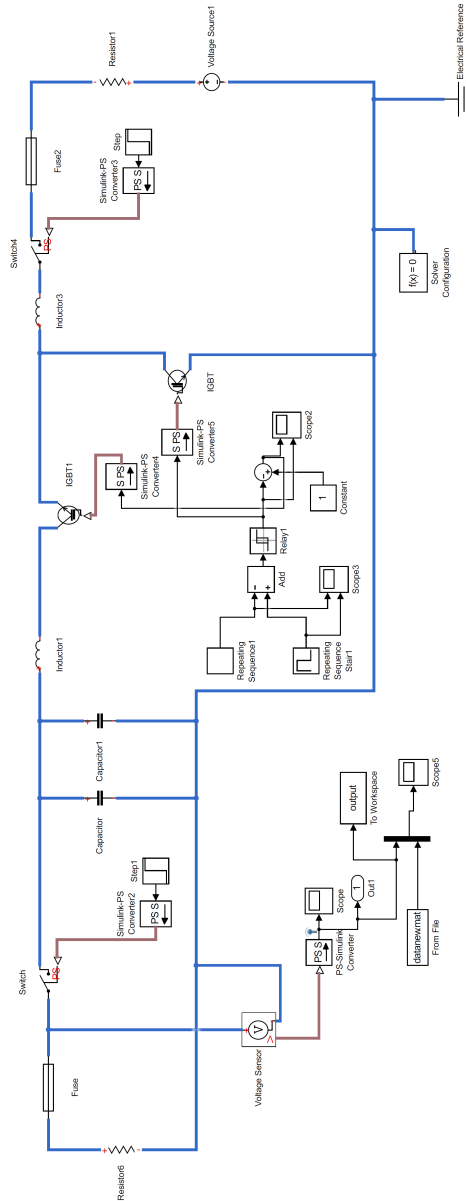


Figure C-1: Wiring diagram of the Power Electronics panel



# APPENDIX D

## DETAILED SIMULINK MODELS



**Figure D-1:** Simulink model for the parameter estimation



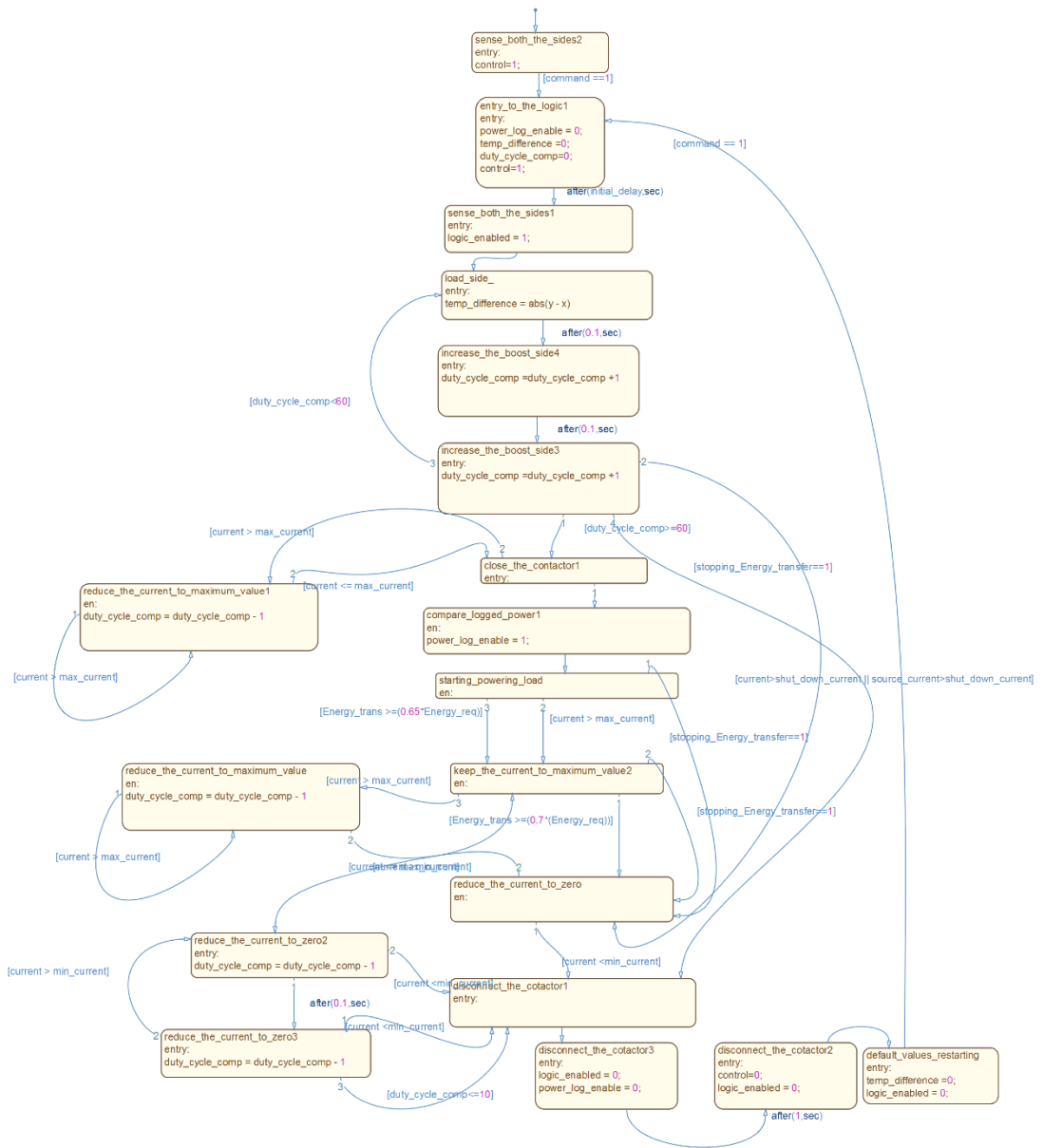


**Figure D-3:** The sequential logic circuits diagram of the  
MATLAB state machine in part 4.6

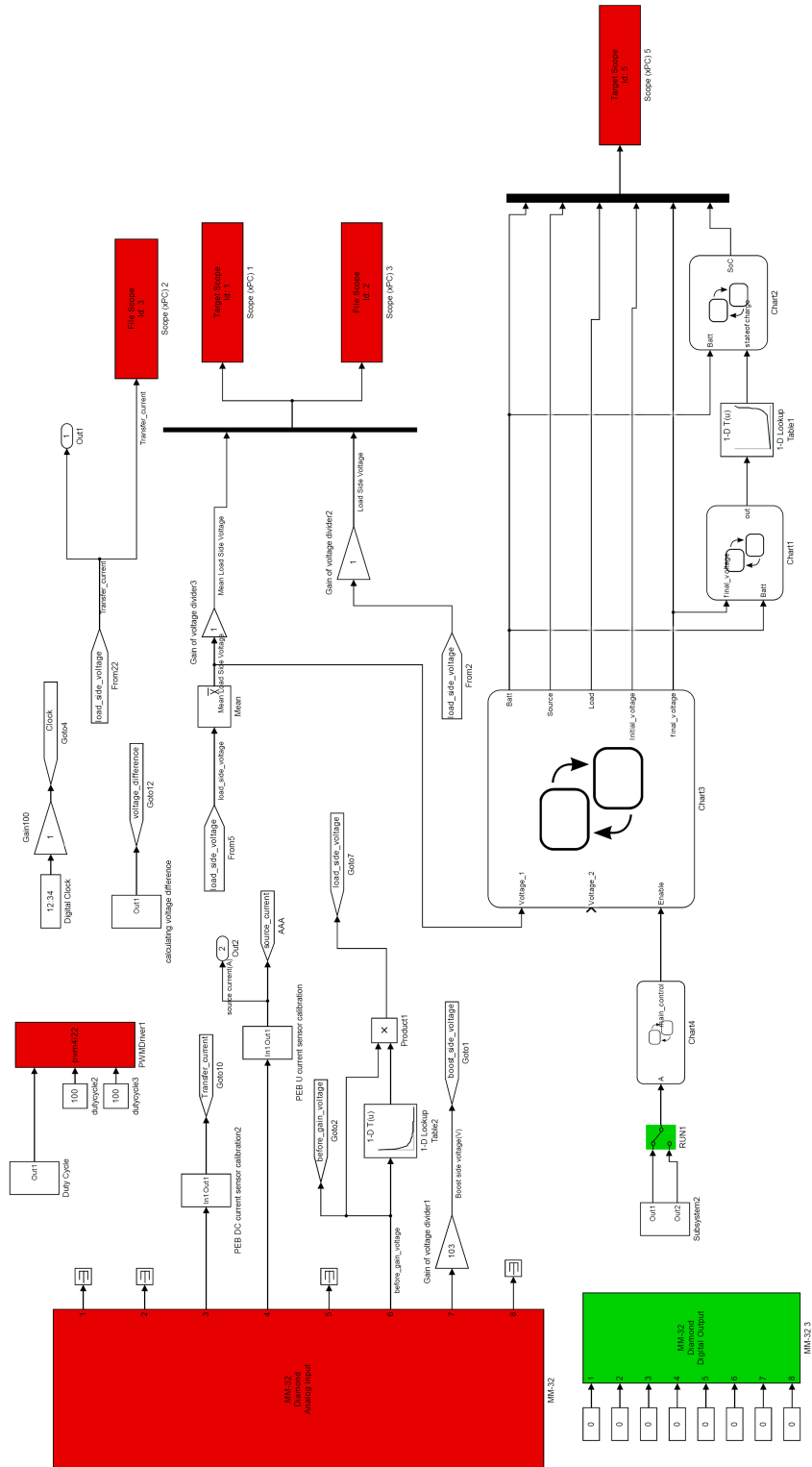


**Figure D-4: Load identification Simulink model**

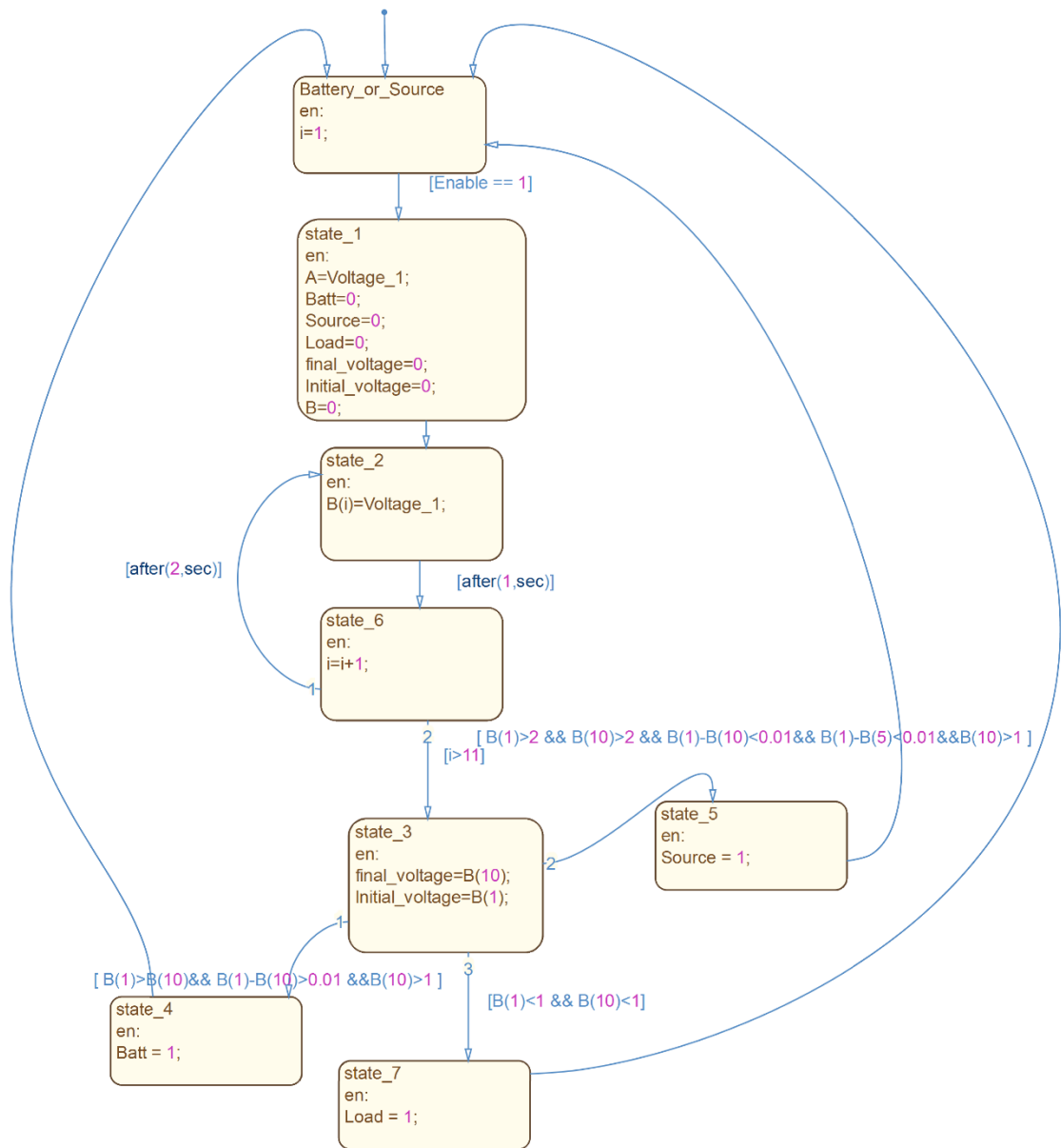


**Figure D-5:** State machine diagram of Chart 1 of the load identification model



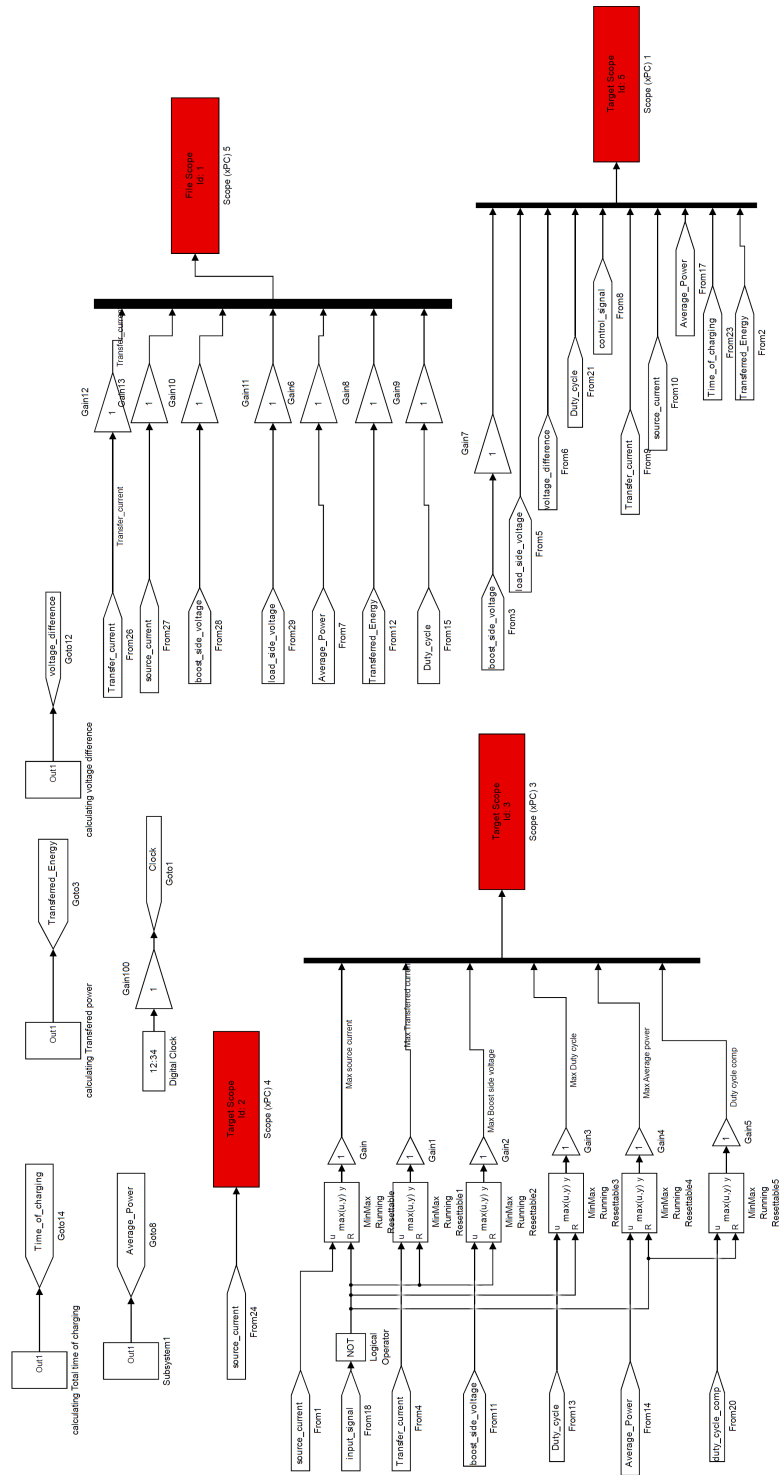


**Figure D-7:** Measurement block of the Simulink model for capturing data and presenting on target PC display





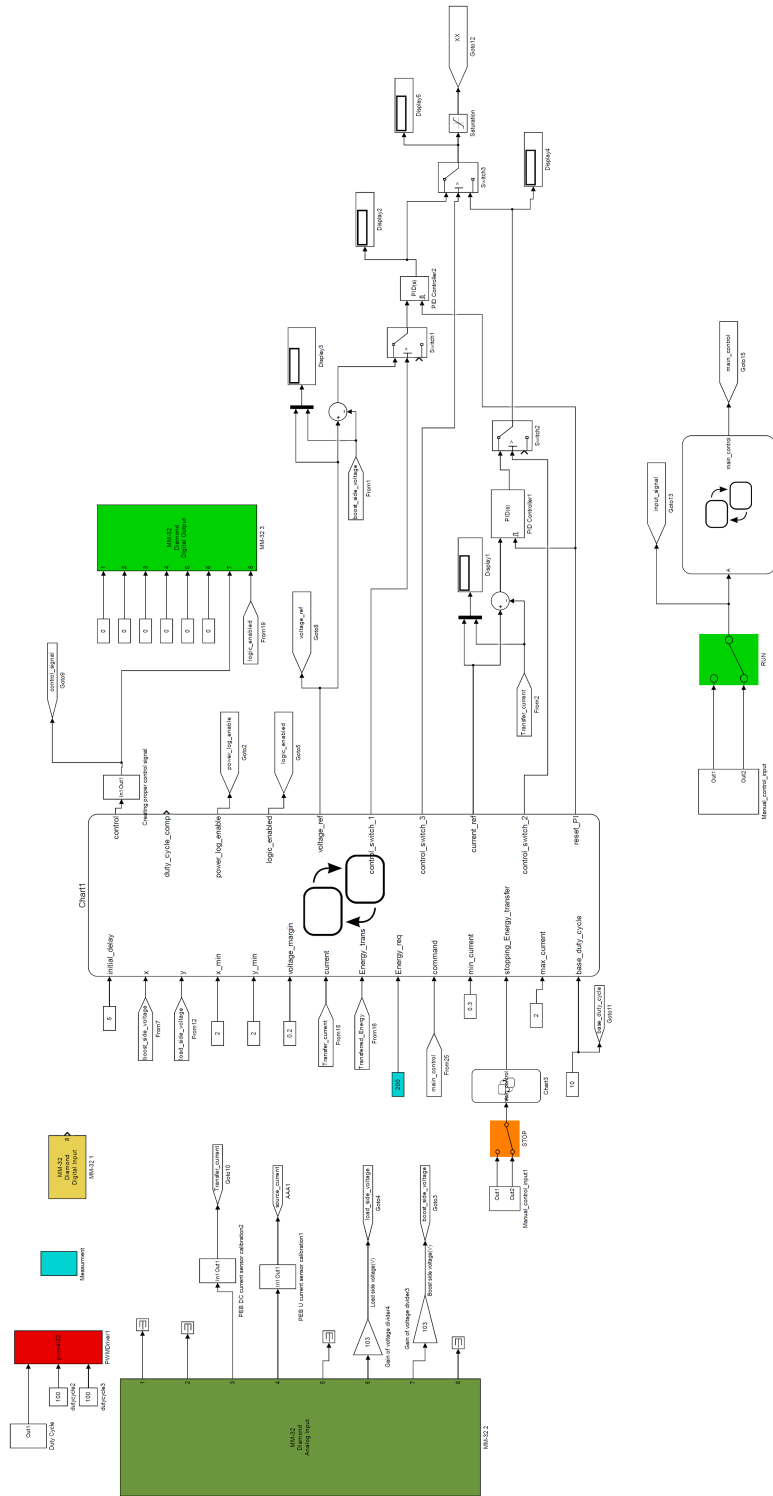


**Figure D-9: Real-Time Simulink model with the PI controllers in the load sharing experiment**

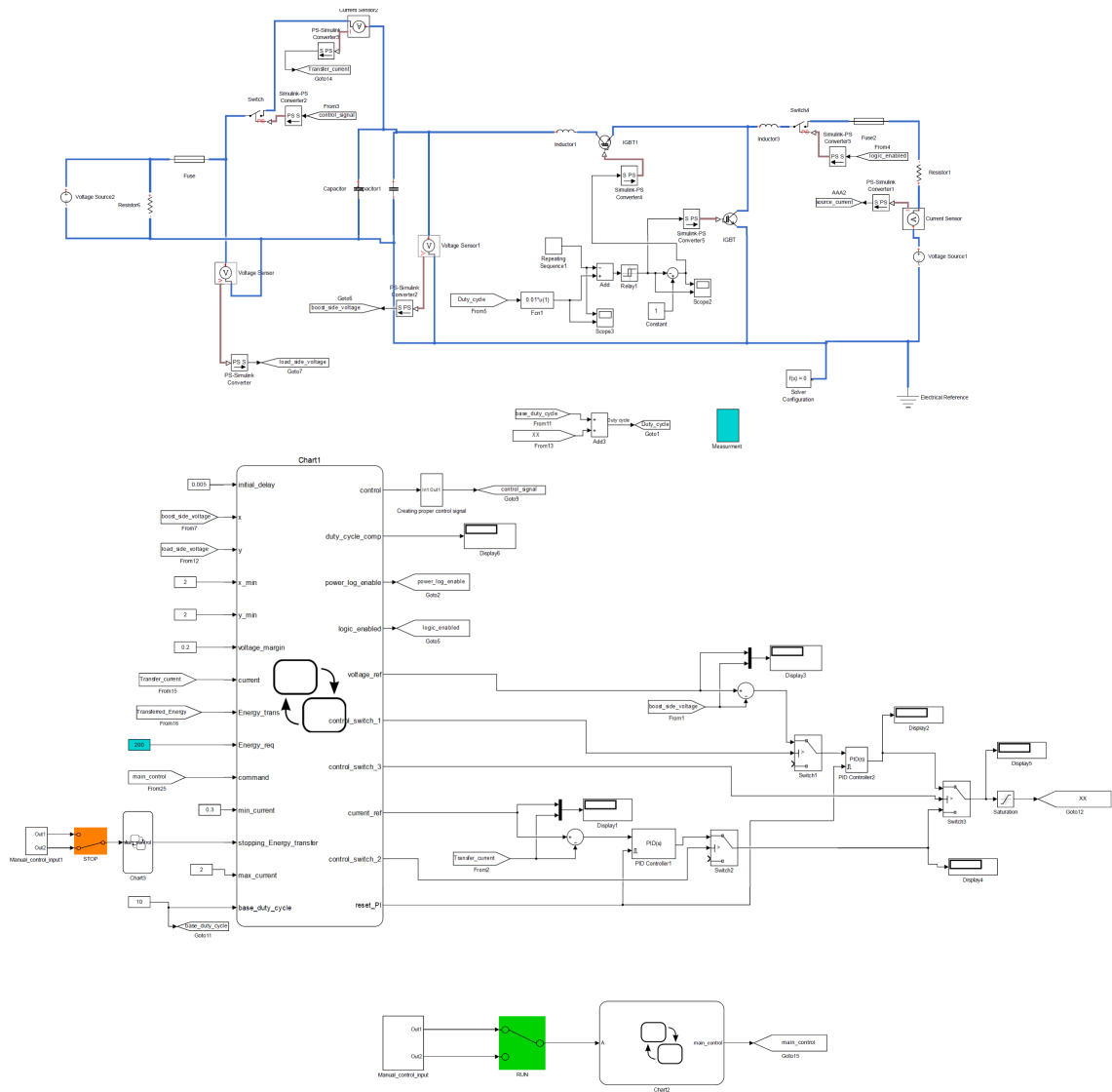


**Figure D-10:** Simulink model of the DC grid and state machine controller  
along with the PI controllers

**Table D-1:** Block parameters of Lead-Acid battery model in MATLAB/Simulink

<b>Nominal Voltage (V)</b>	12
<b>Rated Capacity (Ah)</b>	10
<b>Initial State-Of-Charge (%)</b>	100
<b>Maximum Capacity (Ah)</b>	10
<b>Fully Charged Voltage</b>	13
<b>Nominal Discharge Current (A)</b>	2.5
<b>Internal Resistance (<math>\Omega</math>)</b>	0.015
<b>Capacity (Ah) @ Nominal Voltage</b>	4.5
<b>Exponential Zone Voltage (V)</b>	12.3
<b>Exponential Zone Capacity (Ah)</b>	0.033

# APPENDIX E

## MATLAB CODE FOR PULLING DATA FROM TARGET PC

```
% Pull data from target log files and plot uGrid results
% Initialize
clc
% Get targets objects,
% get target machine objects
tg = SimulinkRealTime.target('TargetPC1');
% set file scope to collect run o fdata
dt=0.001; % target update rate
dec=10; % decimation of data on target
runtime=100;
numsamp=runtime/(dt*dec); % number of samples to collect
scope_obj1 = getscope(tg, 3);
scope_obj1.Decimation = dec;
scope_obj1.NumSamples = numsamp;

% start the targets
start(tg);
% Display ..... and .... durring run
sid_I = getsignalid(tg, 'Gain7');
sid_clk = getsignalid(tg, 'Gain100');
k=1;
timeout=100;% set timeout limit for HIL load run to start
while k<100
current(k)=round(getsignal(tg, sid_I));
t(k)=round(getsignal(tg, sid_clk));
k=k+1;
% plot run updates
    plot(t-t(1),current)
    axis([0, runtime, min(current)*0.95, max(current)*1.05])
%     title(['I = ',num2str(current(k)), ' A'])
    ylabel('A')
    xlabel('time (s)')
%     pause(1)
end
% stop targets before file is accessed
stop(tg);
% copy logdata file to host workspace
SimulinkRealTime.copyFileToHost('D:\LOGDATA.DAT')
% Get data 1
h=fopen('LOGDATA.DAT');
data=fread(h);
fclose(h);
logtg=SimulinkRealTime.utils.getFileScopeData(data);
current=logtg.data(:,1);
```

# APPENDIX F

## POWER BOARD ENERGY EFFICIENCY

The power electronics converter is a required part of a microgrid. By increasing the number of converters in the power system, the efficiency evaluation comes up in terms of efficient grids. The presented converter topology as a boost converter is tested under different load conditions for deriving efficiency values. In this test procedure, the duty cycle is kept at 50% and input voltage changed from 5 V to around 115 V. The input power variation ranges were 2 W up to 1000 W while the resistive load was 41  $\Omega$  for powers below 700 W and 70  $\Omega$  in higher power cases.

**Table F-1:** Power electronics board efficiency in different voltage and current levels

Input Voltage (V)	Input Current (A)	Input Power (W)	Output Voltage (V)	Output Current (A)	Output Power (W)	Efficiency (%)
4.960	0.350	1.736	6.560	0.167	1.096	63.106
14.870	1.270	18.885	24.920	0.632	15.749	83.397
24.770	2.280	56.476	44.650	1.131	50.499	89.418
34.710	3.270	113.502	63.400	1.605	101.757	89.652
44.640	4.180	186.595	81.450	2.067	168.357	90.226
54.580	5.230	285.453	101.080	2.558	258.563	90.580
64.490	6.220	401.128	119.720	3.025	362.153	90.284
74.200	7.270	539.434	139.100	3.531	491.162	91.051
99.100	7.660	759.106	188.730	3.704	699.056	92.089
104.100	8.050	838.005	198.310	3.886	770.633	91.960
114.100	8.830	1007.503	218.130	4.265	930.324	92.340

As seen in Figure F-1, the efficiency versus the input power and the load current increased in the range of power that the power electronics board tested. As expected, the efficiency in low powers is too low for this converter which is related to the IGBT losses. The losses in IGBT and Diode consists of three terms - conduction losses, switching losses, and blocking (leakage) losses. Additionally, there are some other factors, such as losses due to ripple current or diode reverse recovery charge loss which can make the loss calculations very complicated as presented in [50, 51]. In all of the regulators, efficiency for low power (current) is less than that related to the working point of the converter.

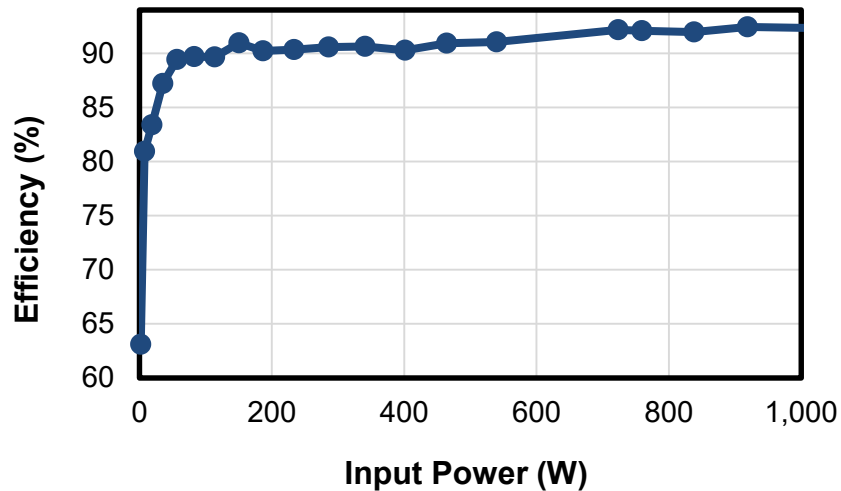


**Figure F-1:** Power board efficiency versus input power

As seen in Figure G-17, this power board shows that the efficiency for small outputs is less than 80% while it is more than 90% for all other test points.

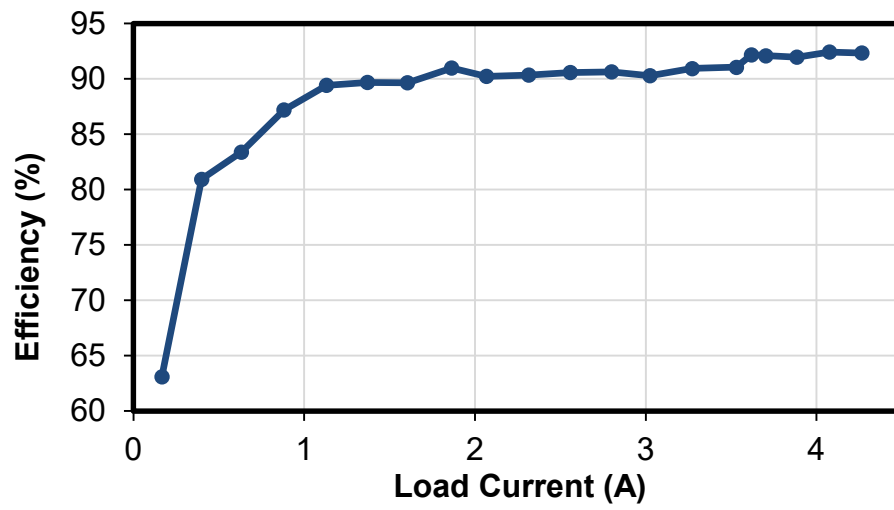


**Figure F-2:** Power board efficiency versus output current

# APPENDIX G

## VOLTAGE SENSORS CALIBRATION

This experimental setup is able to make any microgrid reach up to 400 V on the high-side bus. The Printed Circuit Board (PCB) of the converter already has some voltage and current sensors which are used to measure phase voltages and currents. As the load identification system needs to measure voltage before connecting to the converter, a voltage sensing board is also installed on the experimental setup. The voltage sensing board consists of voltage divider resistors along with op-amps and Zener diodes. The input range of the sensing voltage board could up to 400 V and the output range is under 5 V at all times. This limit is due to the limitations of the analog input ports of digital hardware.

The voltage gain for changing the sensing voltage to real voltage varies according to the input range. This means that the constant voltage gain is not useful while the board is working on different voltage levels. The lookup table was created according to the experimental results and then implemented in the real time MATLAB/Simulink model. In Figure H-1, the gain values versus input voltage range shows.



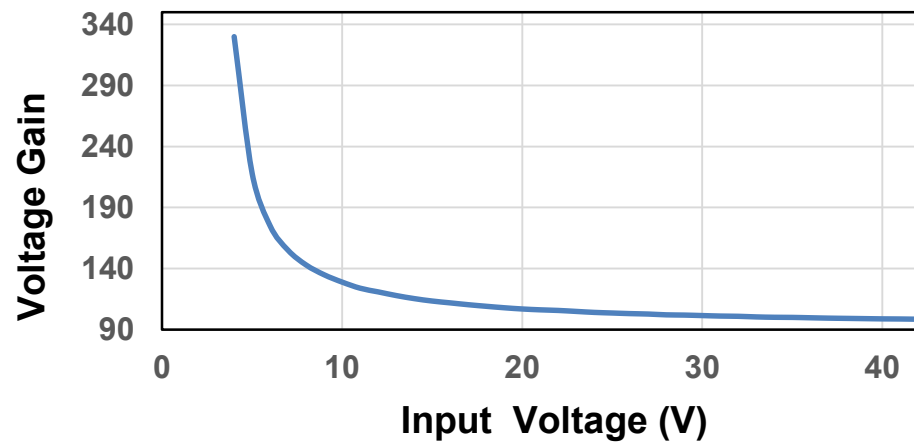


**Figure G-1:** Voltage gain value of the voltage sensing board versus input voltage